The Abdus Salam
International Centre for Theoretical Physics

United Nations
Educational, Scientific and
Cultural Organization

IAEA
International Atomic Energy Agency

1936-51

Advanced School on Synchrotron and Free Electron Laser Sources and their Multidisciplinary Applications

7 - 25 April 2008

X-ray imaging: absorption, phase contrast and tomography

Giuliana Tromba
Sincrotrone
Trieste

X-ray imaging: absorption, phase contrast and tomography

Giuliana Tromba

Sincrotrone Trieste

SYRMEP beamline

(SYnchrotron Radiation for MEdical Physics)

Outline

- Advantages of SR for X-ray imaging
- Absorption and Phase Contrast imaging
- The SYRMEP beamline: source characteristics and experimental setup
- Some applications

Advantages of SR for hard X-ray imaging

Characteristics	Advantages
Monochromaticity	no beam hardening k and L edge imaging quantitative CT evaluations optimization of X-ray energy (dose reduction)
Collimation	parallel beams, scatter reduction
Spatial coherence	phase sensitive techniques
Intensity	reduction of exposure time

PHase-Contrast (PHC) imaging

The technique exploits the high spatial coherence of the X-ray source

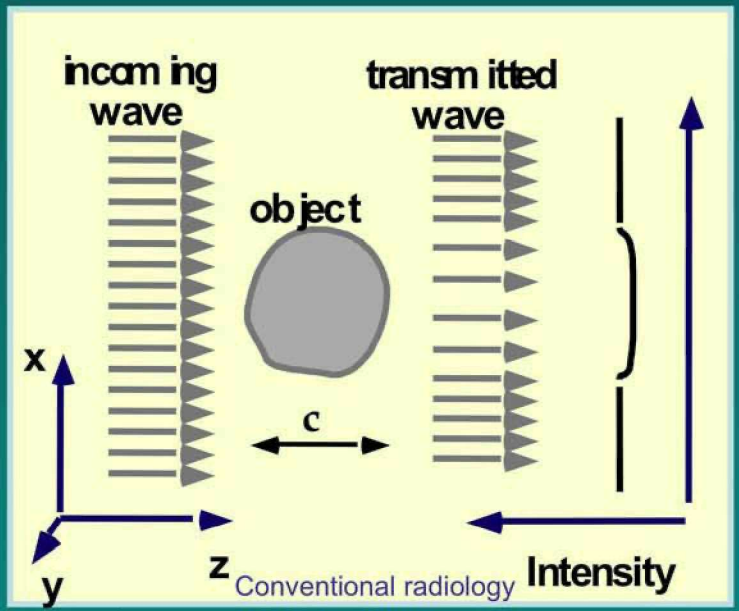

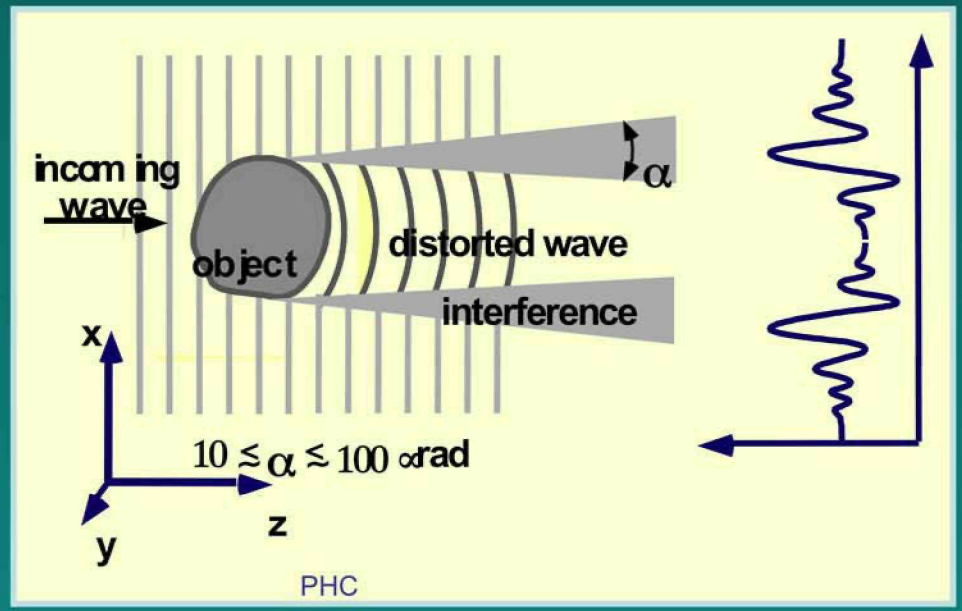

$$(\Delta I/I)_{abs} = e^{\,c\,\Delta\mu} - 1$$

$$\Delta\phi = 2\pi\, c\, \Delta\delta / \lambda$$

$\mathbf{n} = 1 - \delta - i\beta$: refraction index

$\mu = 4\pi\,\beta / \lambda$: linear absorption coeff.

c : object size // to beam direction

In conventional radiology image formation is based on differences in X-ray absorption properties of the samples. The image contrast is generated by density, composition or thickness variation of the sample. Main limitation: poor contrast in soft tissue differentiation.

***Phase sensitive* techniques** are based on the observation of the *phase shifts* produced by the object on the incoming wave. Contrast arises from interference among parts of the wave front differently deviated (or phase shifted) by the sample. Edge enhancement effects.

PHC imaging setup

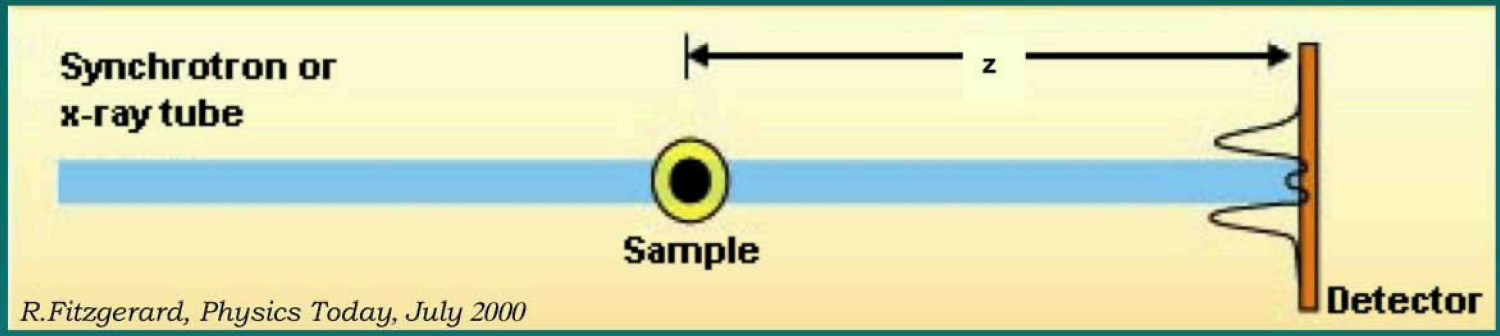

- z =0 -> absorption image
- For z > 0 -> interference between diffracted and un-diffracted wave produces edge and contrast enhancement. A variation of δ, producing a phase shift, can be detected
- Measure of $\nabla^2\Phi(x,y)$

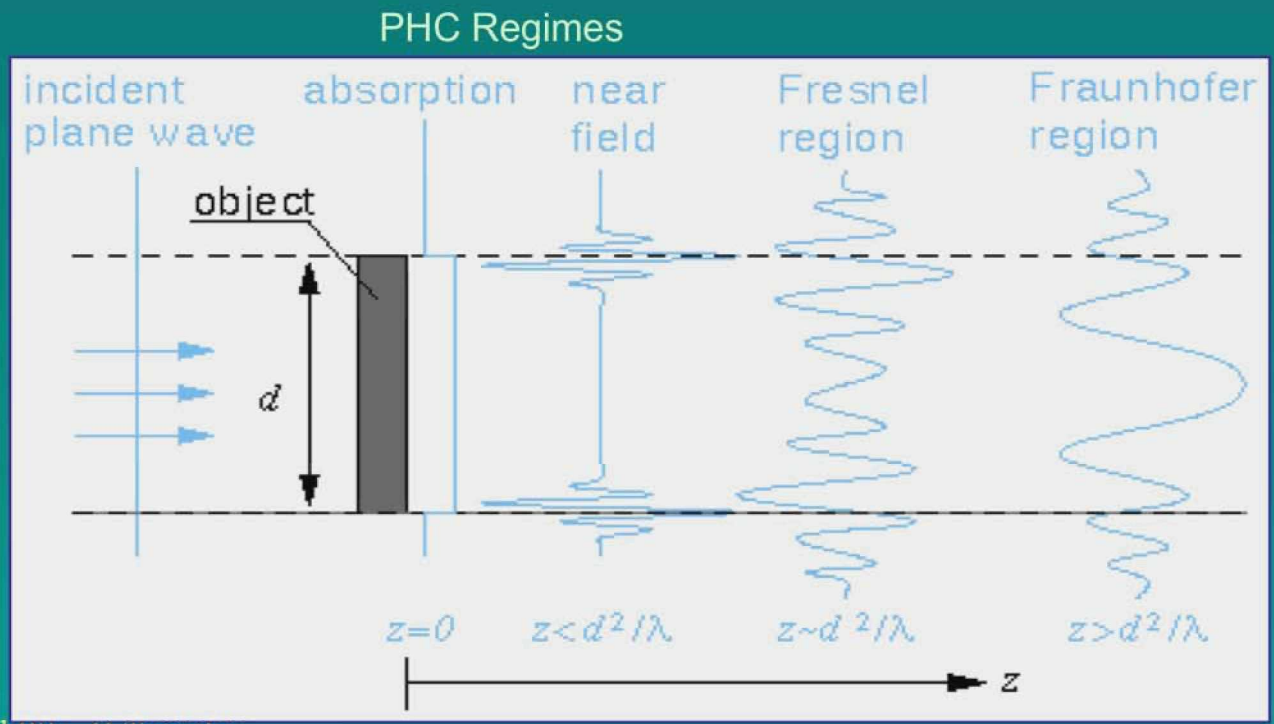

PHC vs. Absorption

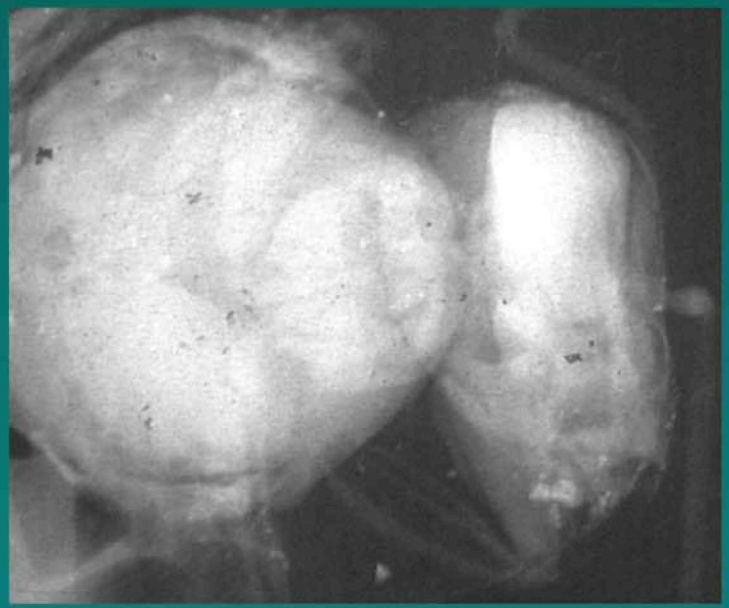

10 keV

Absorption

Phase Contrast

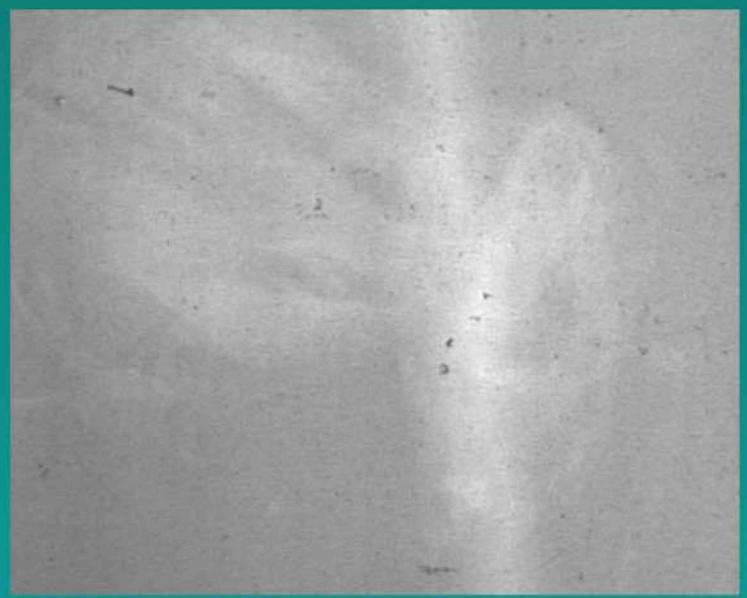

20 keV

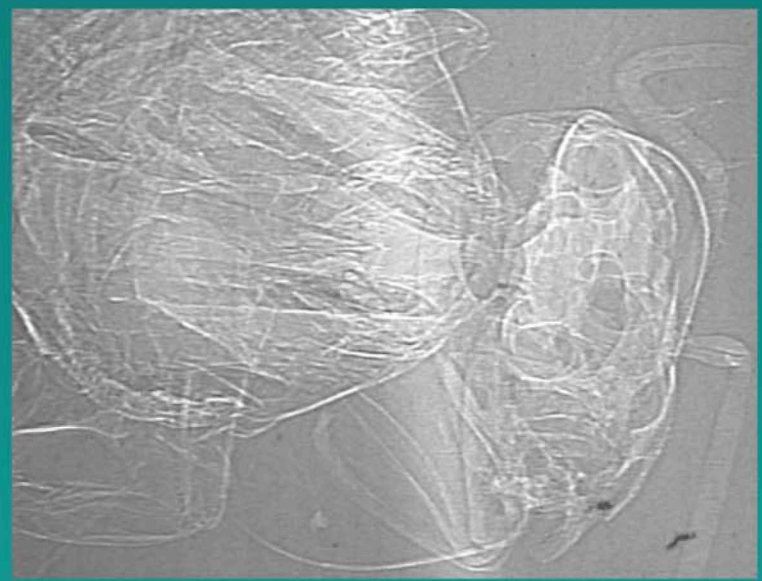

SYRMEP layout and source characteristics

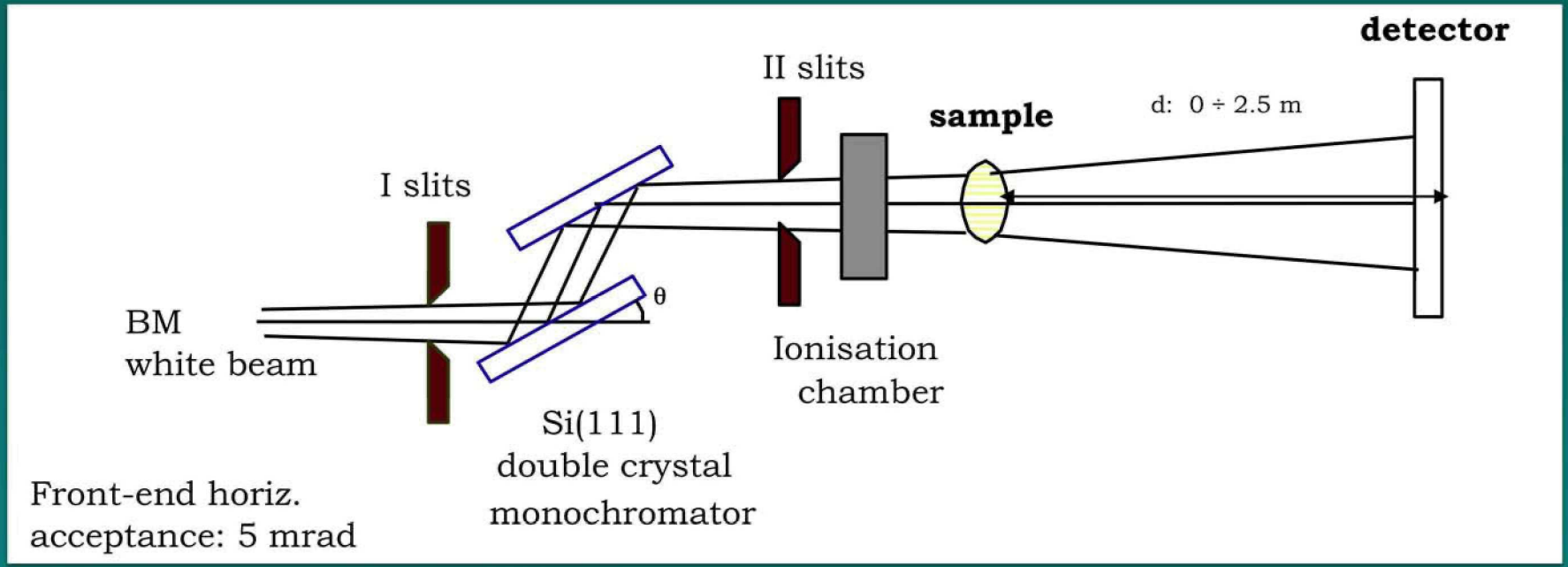

- Source size ≅ 100 μm x 1100 μm
- Source-to-sample distance ≅ 23 m
- Sample-to-detector distance d: 0 ÷ 2.5 m
- Energy range: 8 ÷ 35 keV, Bandwidth $\Delta E/E \cong 10^{-3}$
- Typical fluxes at 15 keV ≅ $2 * 10^8$ phot./mm^2 s (@ 2 GeV, 300 mA)
  $7 * 10^8$ phot./mm^2 s (@ 2.4 GeV, 180 mA)
- Transverse coherence length at 15 keV ($Lc = \lambda L / 2*\sigma$) ≅ 10 μm
- CCD (2048*2048 pixels) 16 bit camera with 2 configurations:
  - pixel size: 14 μm, 1:1 optical fiber taper, field of view: 28.67x28.67 mm^2
  - pixel size: about 3.8 μm, with high resolution optics, field of view of about 8 mm^2.
- CCD (4008*2672 pixels) 12/16 bit camera
  - pixel size: 9 μm, 1:2 magnifying optics (4.5 μm effective pixel size, field of view ≅: 18x12 mm^2

Simulated PHC patterns for a 100 μm nylon wire

Influence of:

- Source dimension
- Sample-to-det. distance
- Detector resolution

Source dimension

Distance sample-detector

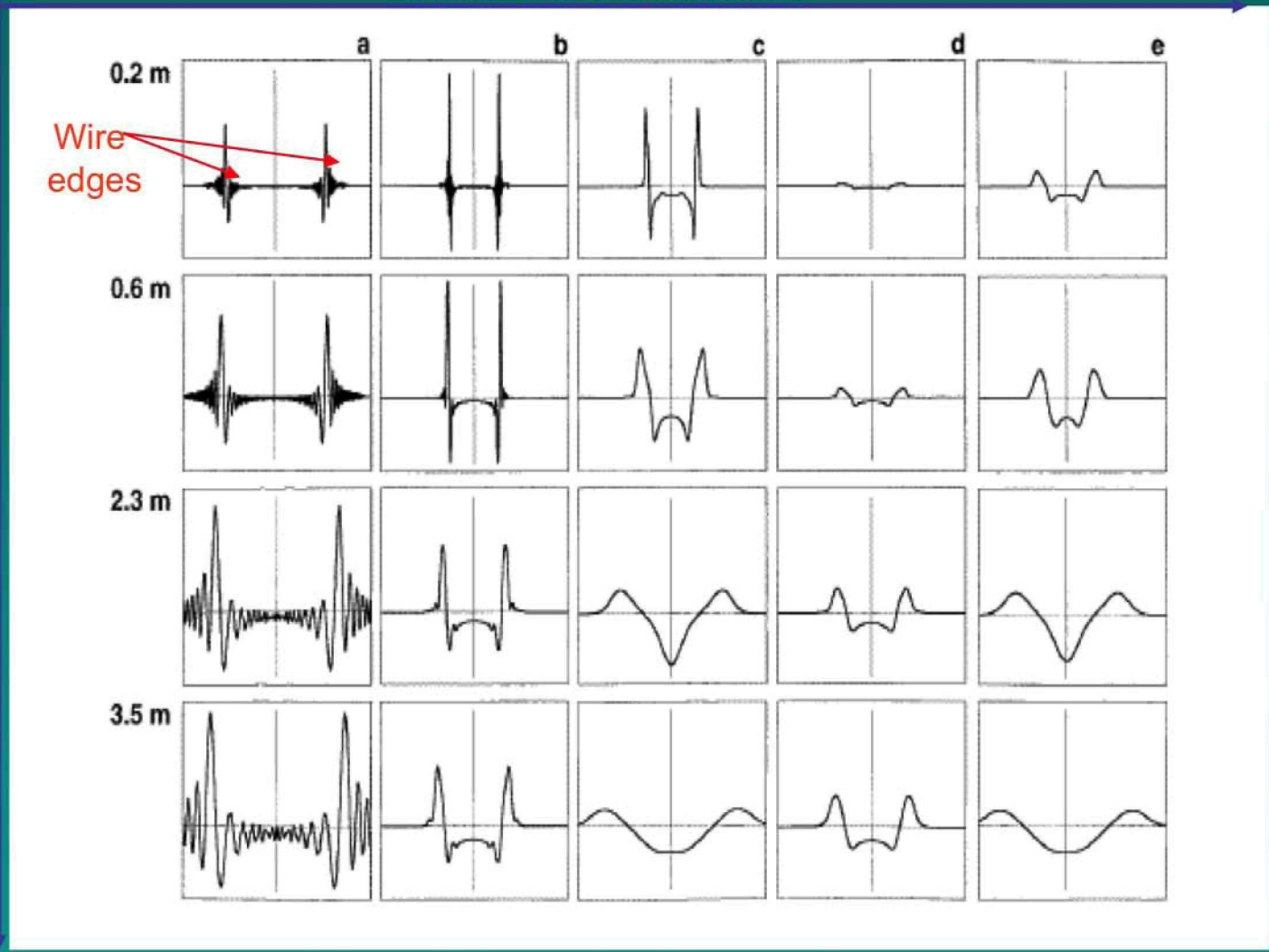

Point 140 μm 1100 μm 140 μm 1100 μm

Ideal detector

Convoluted with 30 μm detector PSF

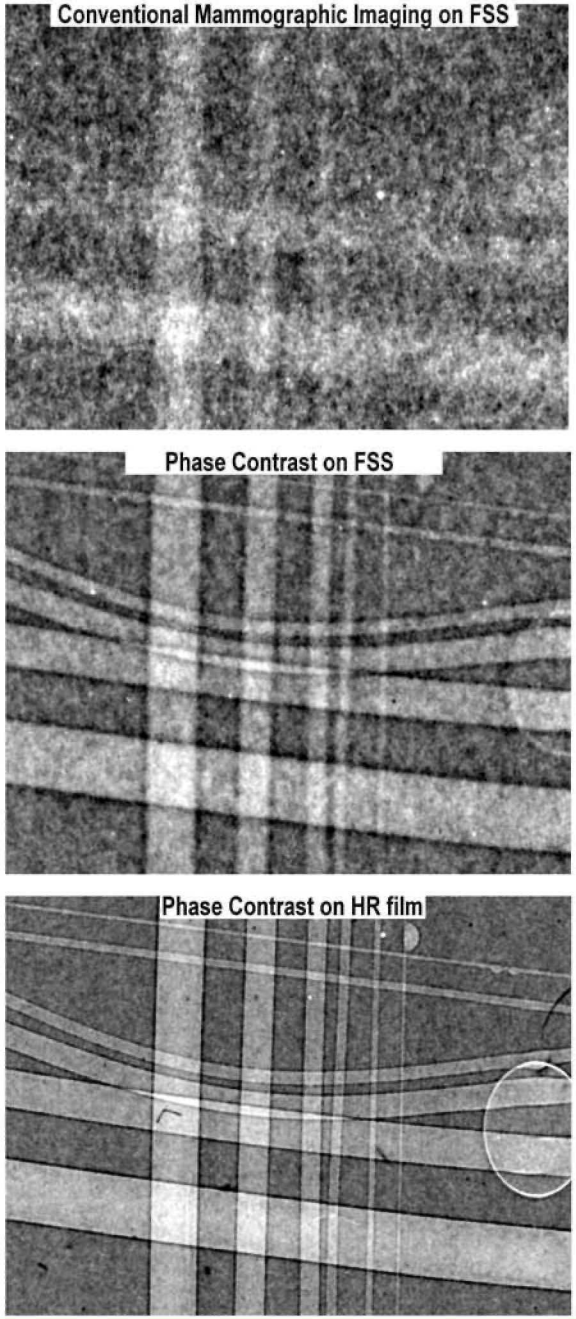

Real images of nylon wires

Application of PHC to the study of sail cloths

Laminates are sailclothes in which some cloth or yarns are glued to one or more layers of films, where some attempt is made to align the load bearing fibers in a given material with the primary load paths

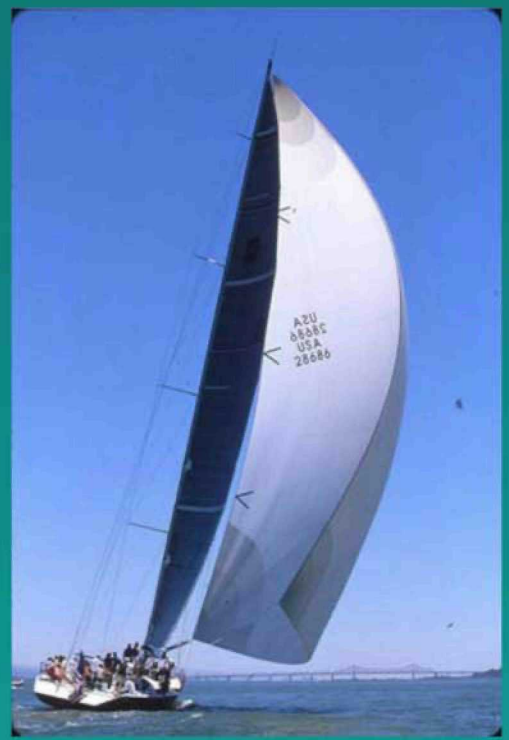

Cuben Fiber **laminates use unidirectional prepreg tapes of in-line plasma treated extended chain polymer fibers, and carbon, spread to monofilament levels on polyester and other unique films. The beauty of the CF process is that it involves neither twisted filaments nor weaves. This reduces 'creep' and 'crimp' to levels undetectable with standard testing equipment.**

SEM analysis of composites

- Artifacts induced by sample preparation
- Damage induced by vacuum and electron beam
- Limited field of view
- Invasive technique

X-rays?

Poor absorption contrast
Enter PHC

Phase-contrast (d = 66 cm) and absorption (d = 2 cm)

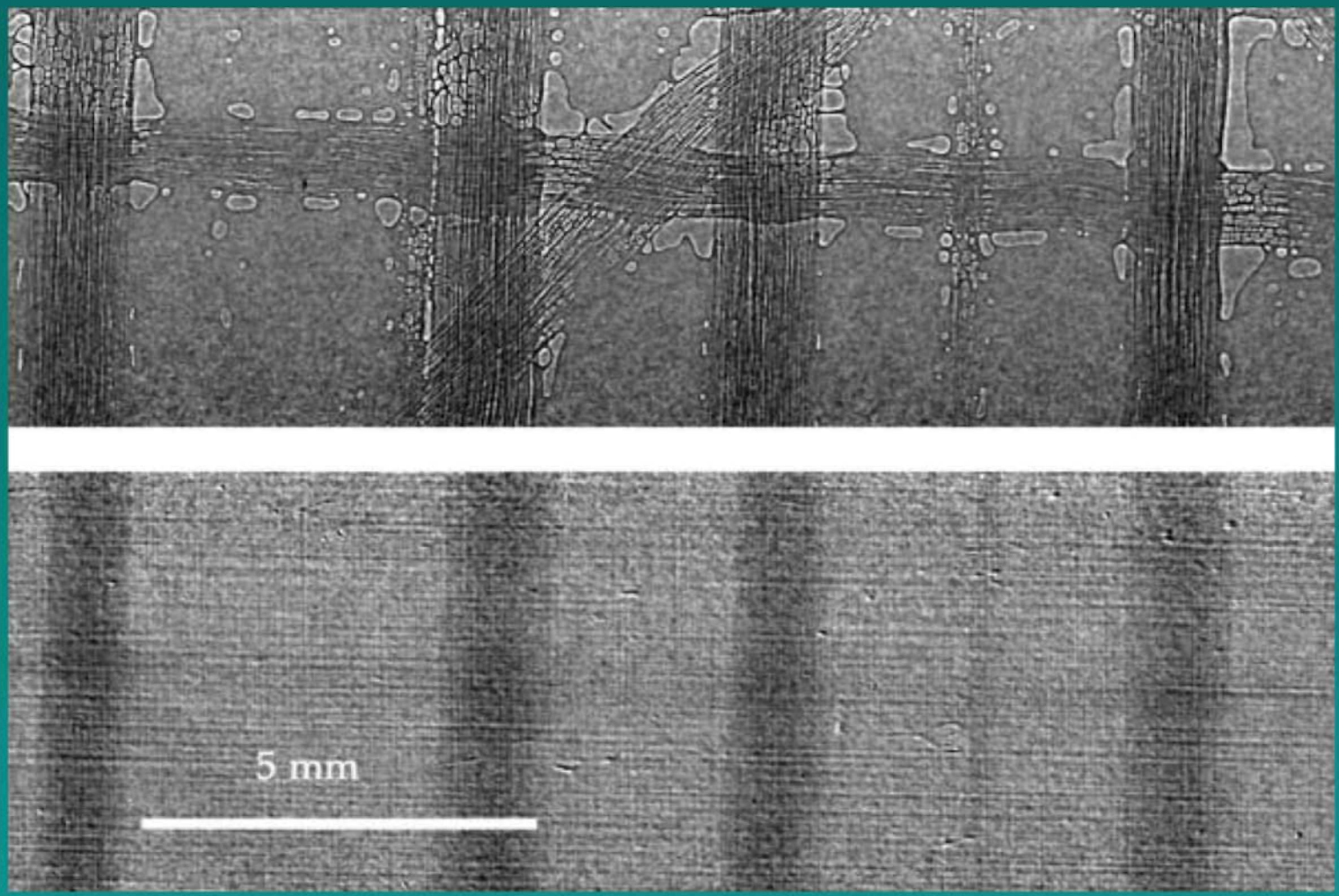

Diax 70 HMT E = 15 keV pixel size = 14 μm

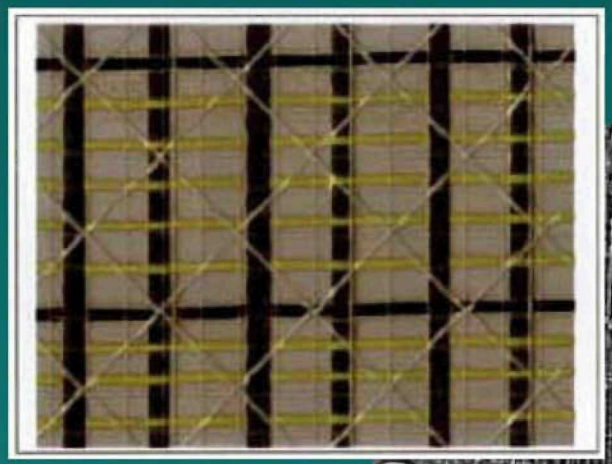

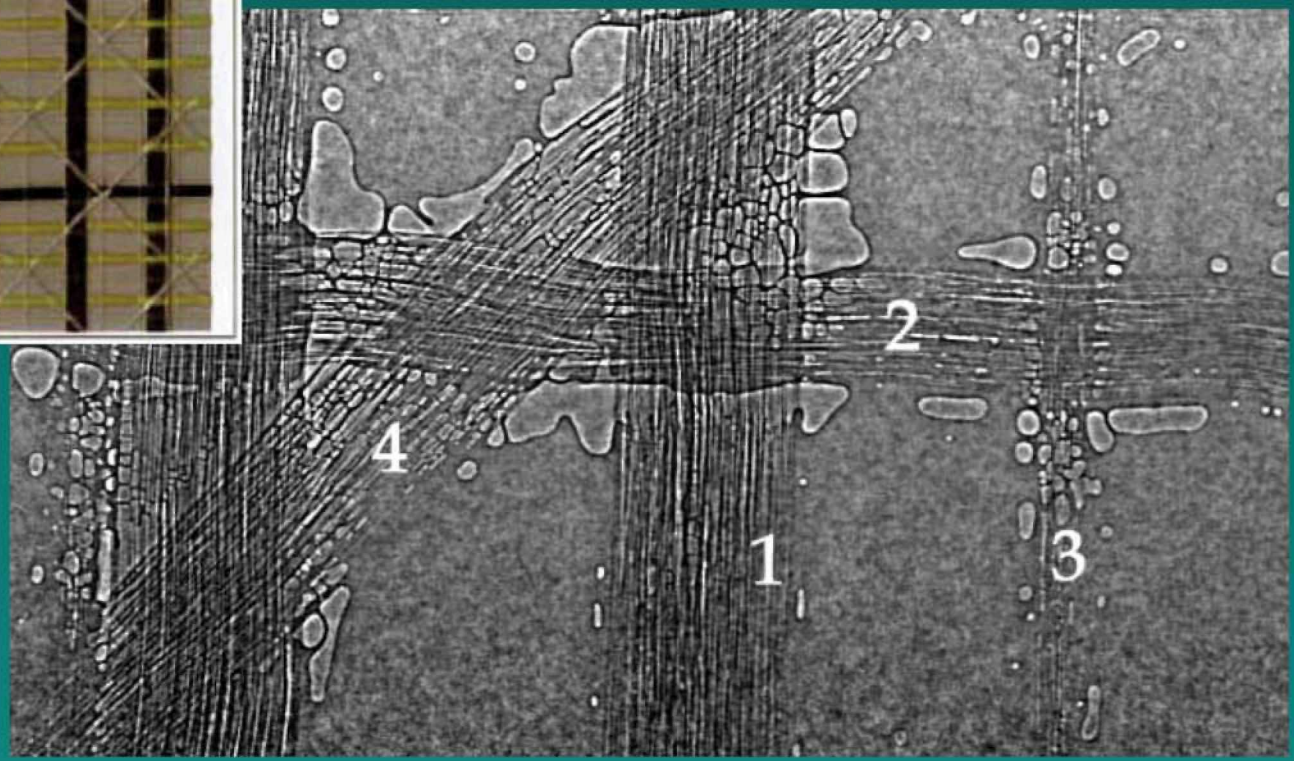

DIAX is Bainbridge's brand name for racing laminates with a 45-degree diagonal scrim.

Optical microscopy vs. x-rays

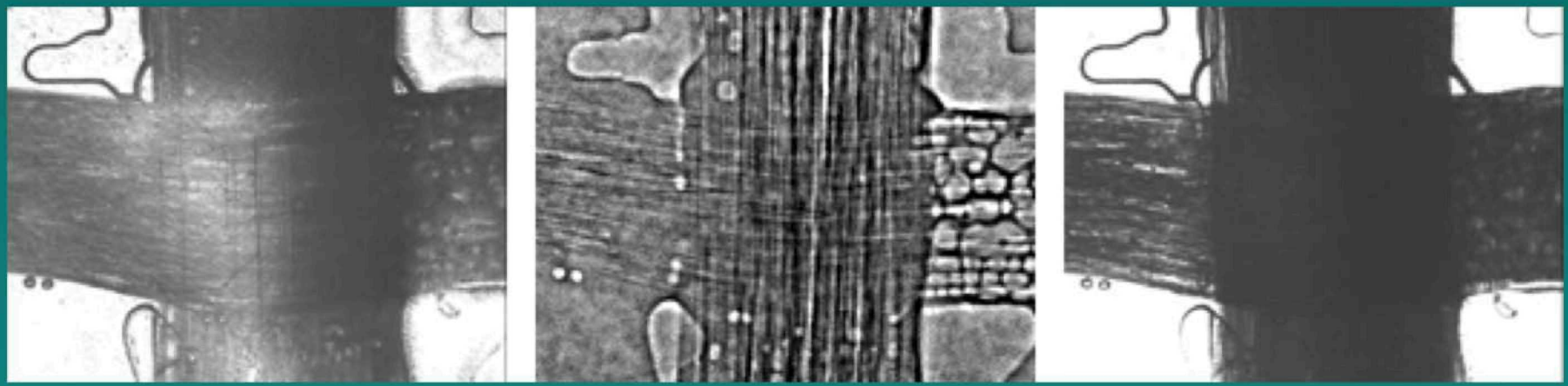

Reflection (left) and transmission (right) optical microscopy have a limited field of view and do not allow observation of details under the ribbons.

Imaging of different sailcloths

cf55

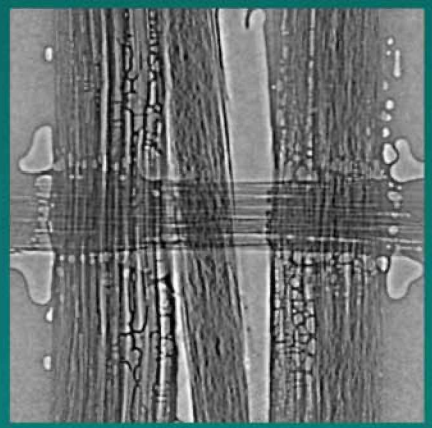

kx14

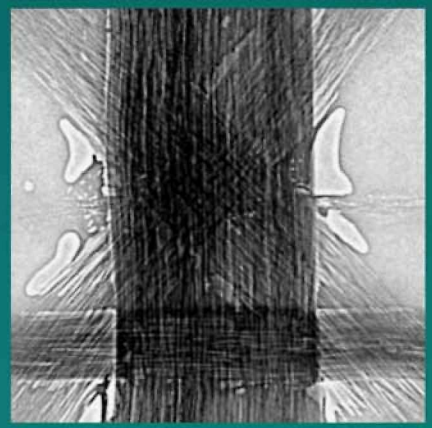

Diax 240p

Diax pp44hmt

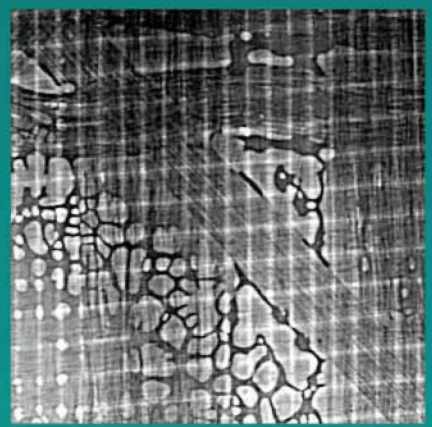

Diax pp130hmt

5 x 5 mm^2
pixel 14 μm

Structural analysis of sailcloth under sailing and racing conditions

- Determination of mechanical parameters in order to predict uniaxial strength, fracture toughness, impact resistance, hygrothermal effect, UV-induced damage.
- Analysis during application of mechanical stress, cycles of flexing and folding, UV irradiation

Impossible or extremely complicated with conventional x-ray imaging systems

Folding cycles on Cuben sailcloth

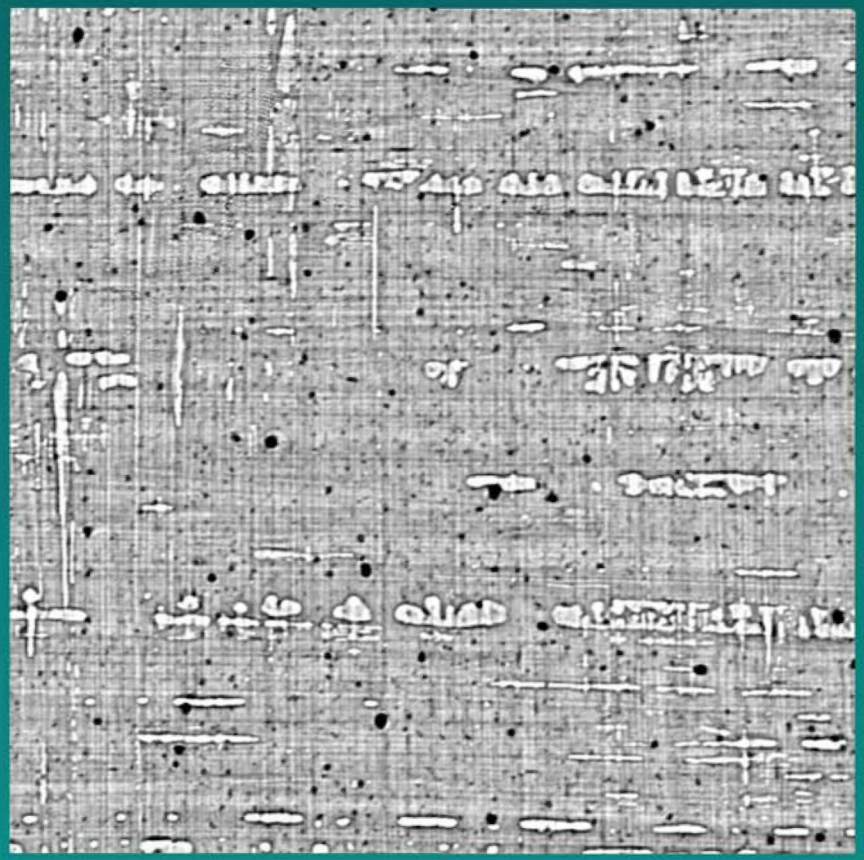

Before folding

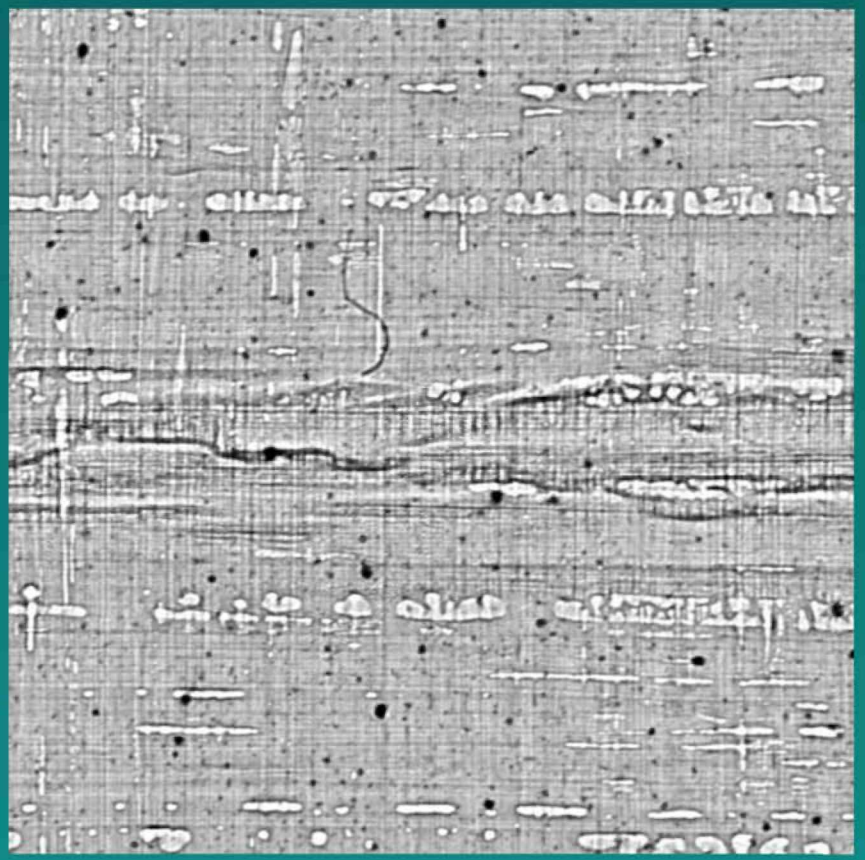

After 60 folds

3 x 3 mm^2 - pixel 3.8 μm

Folding cycles on Cuben sailcloth

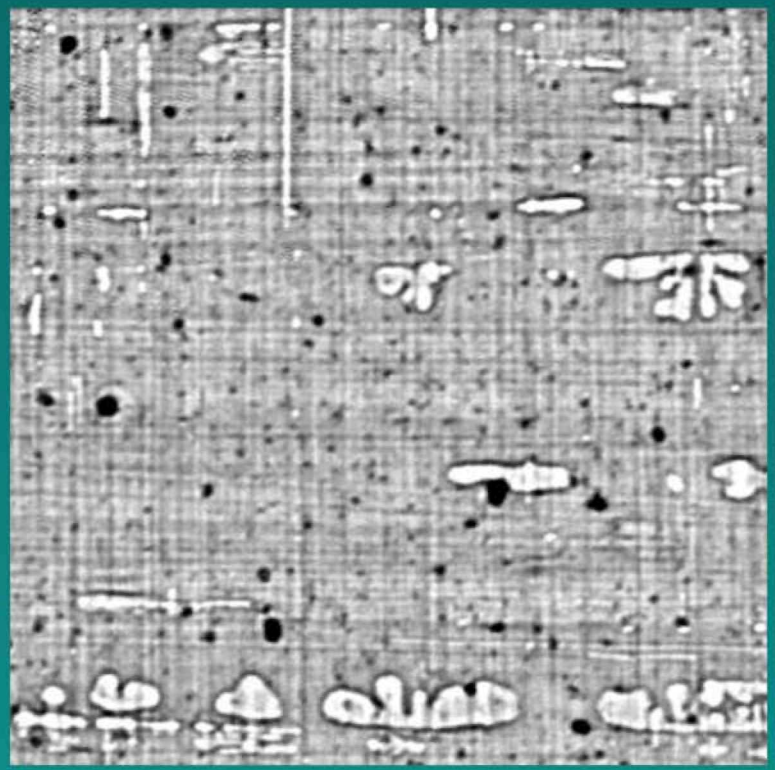

Before folding

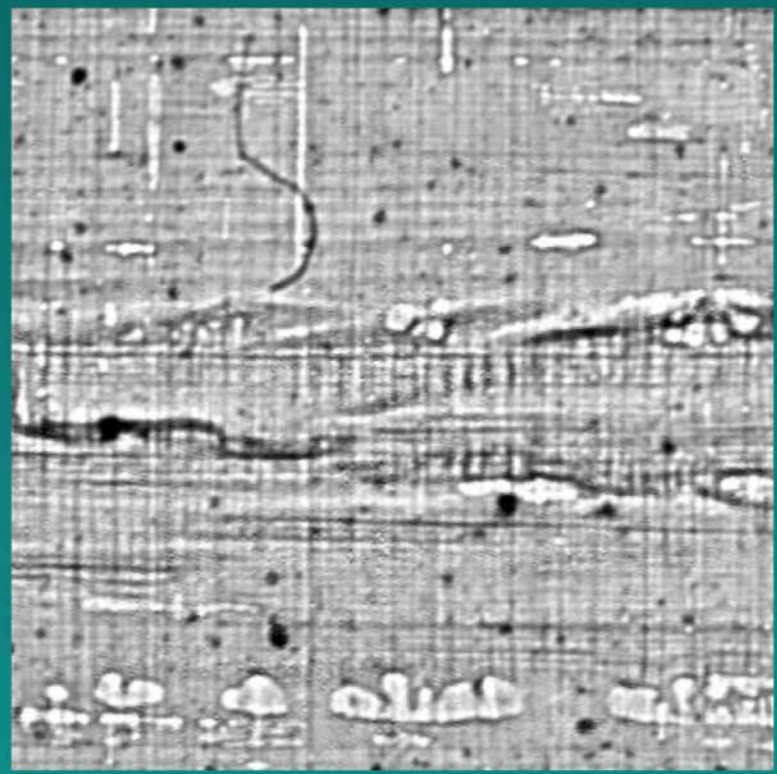

After 60 folds

1.5 x 1.5 mm^2 - pixel 3.5 μm

Folding cycles on laminates

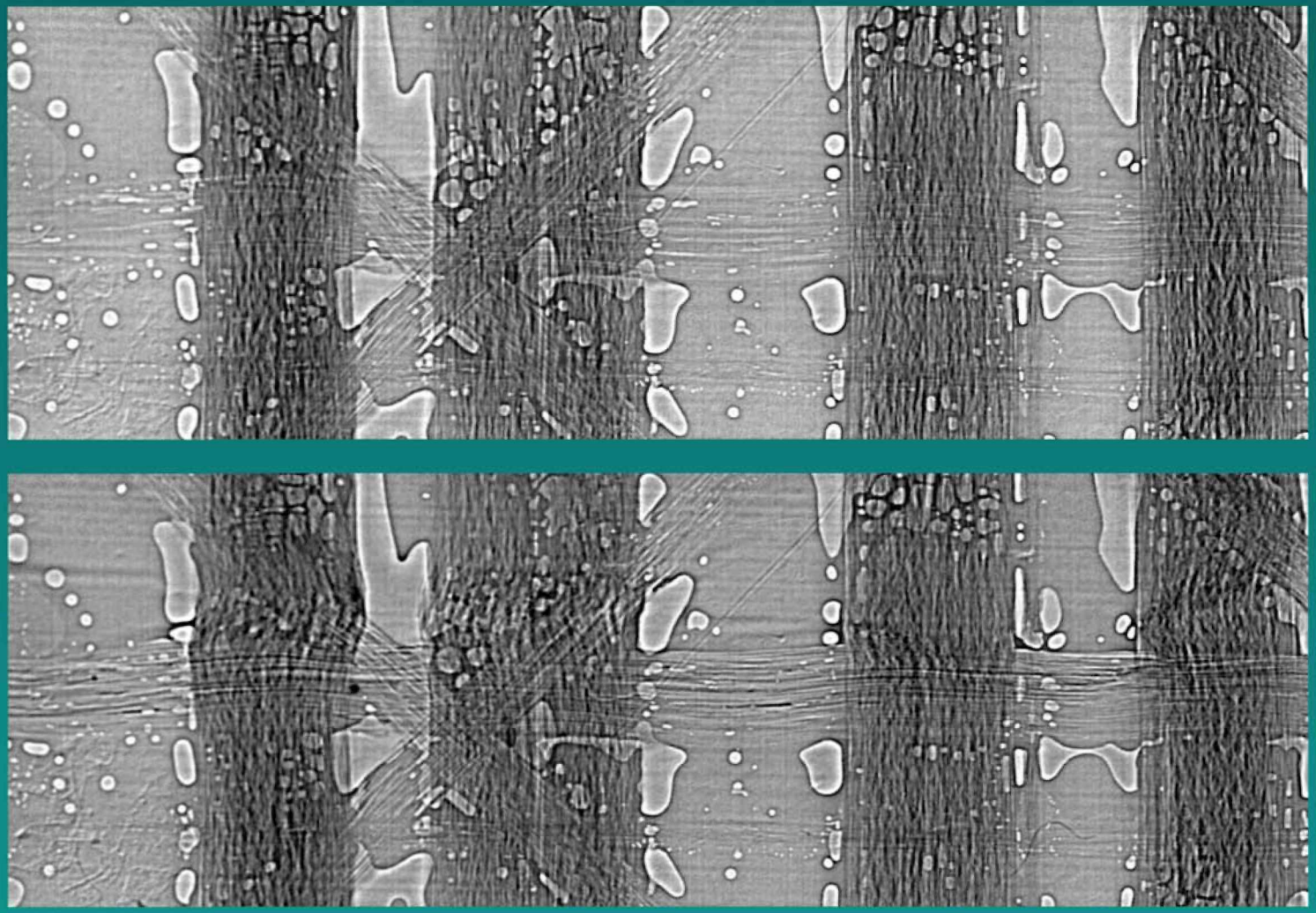

5.6 x 16.8 mm^2 - pixel 14 μm - before folding and after 10 cycles

Folding cycles on laminates

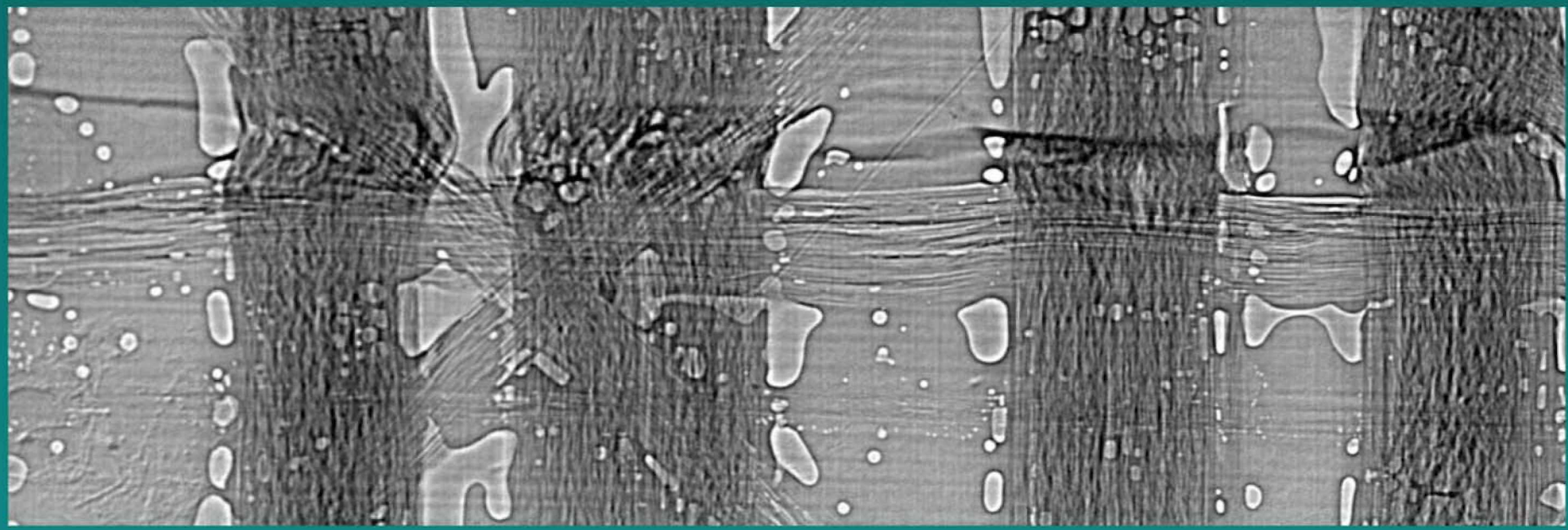

5.6 x 16.8 mm^2 - pixel 14 μm
after 60 cycles

Folding cycles on laminates

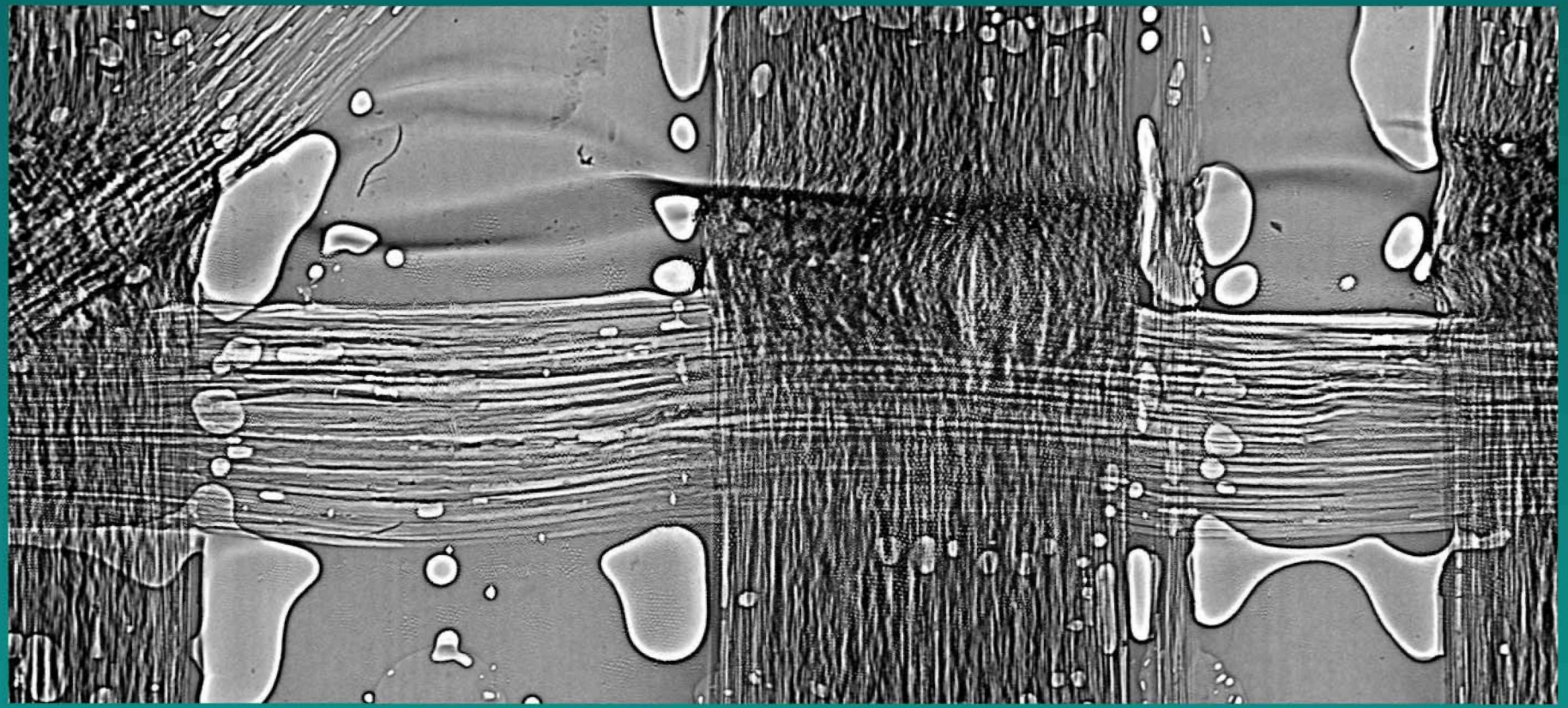

3 x 7 mm² - pixel 3.8 μm
after 90 cycles

Computed μ-Tomography (μ -CT)

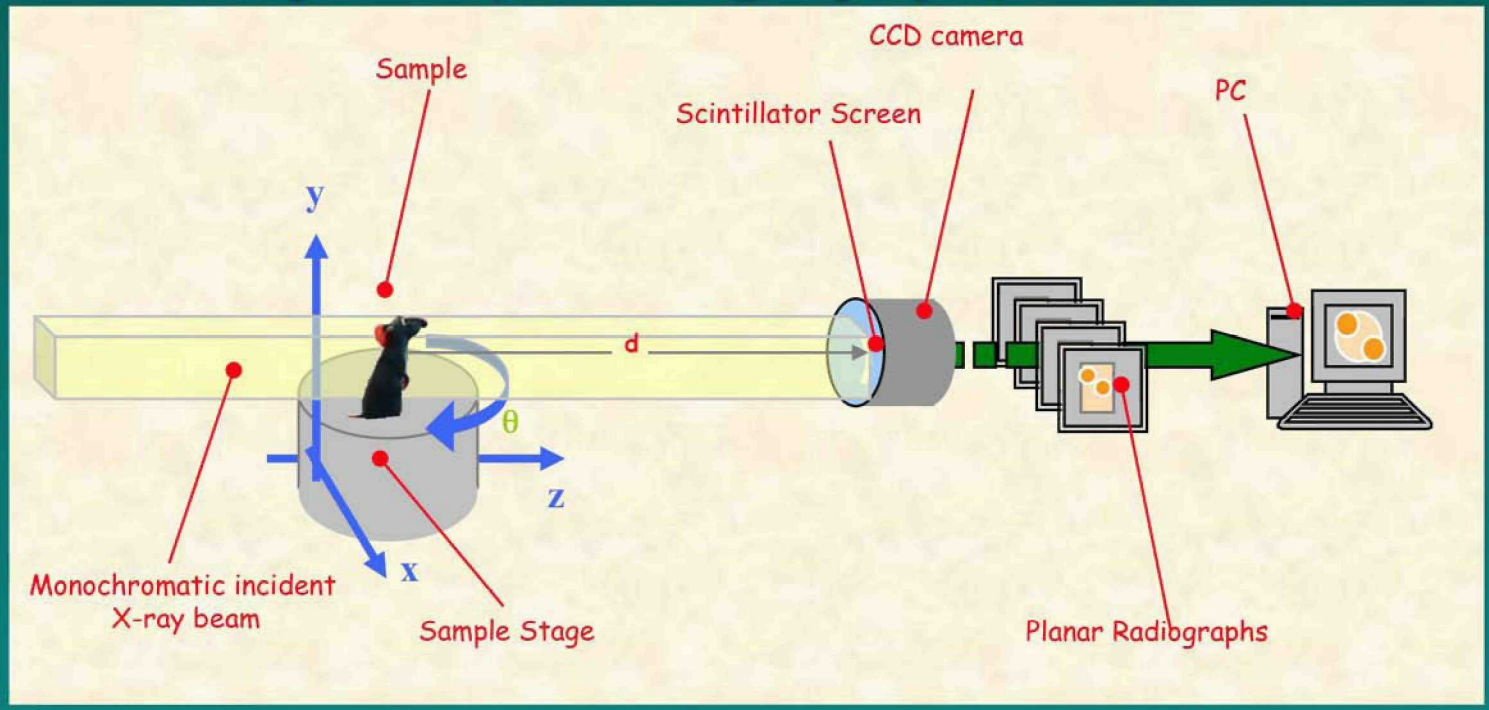

- *In material science: not destructive tool to study the **internal features** of the sample*
  - It dose not require any sample preparation
  - the sample can be after studied by other experimental techniques, or submitted to several treatments (mechanical, thermal, etc...)
  - access to quantitative information on the *density maps* of the irradiated volumes
- *In biomedical imaging: suited for in vivo imaging on small animals (taking into consideration the radiation dose!!)*

- Projections are elaborated by the Filtered Back Projection algorithm (*Herman*, 1980) to reconstruct multiple slices of the scanned sample
- Slices are stacked to create volumes and rendered for visualization
- Volumes can be elaborated by custom adapted Digital Image Processing procedures

Imaging of red calcareous algae

The red calcareous algae (Corallinales) have an essential role in submarine ecosystems:

- bio-builders,
- food for grazers,
- they provide (as bio-builders) calcareous material for the structure of the reef
- part of the Carbon bio-chemical cycle.

Moreover:

- the are widely spatially distributed from warm regions (tropical - temperate) to the cold ones (arctic - subarctic).
- high temporal distribution, from the present (living forms) to the Terziary (Oligocene) fossils thalli.
- high conservative power (paleomarkers)
- used as bioindicator of the quality of the sea waters

Corallinales are considered as an essential tool to access information about submarine environmental evolution

Courtesy of G.Bressan

Aim

Set up a non invasive method that allows a morphologic study of the inner structure of the Corallinales in a resolution scale of 10 μm.

Use this method for virtual slicing the sample and determine where to perform more accurate analysis by means of SEM.

Sample: Rodolith box work

Slice obtained from a 1440 proj.
E= 25 keV

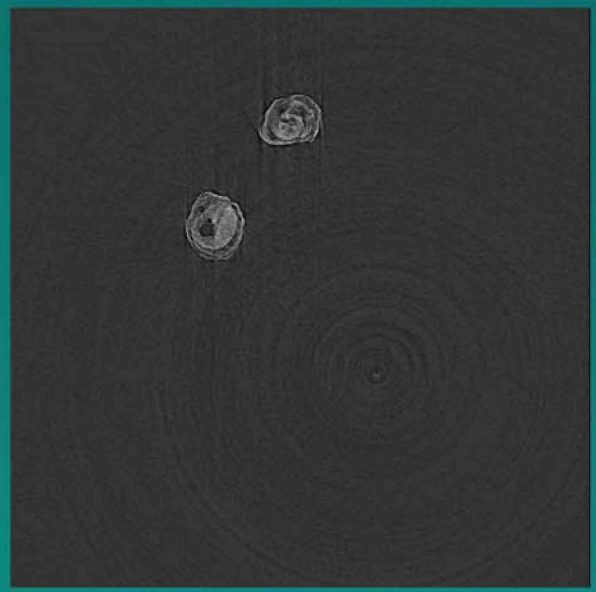

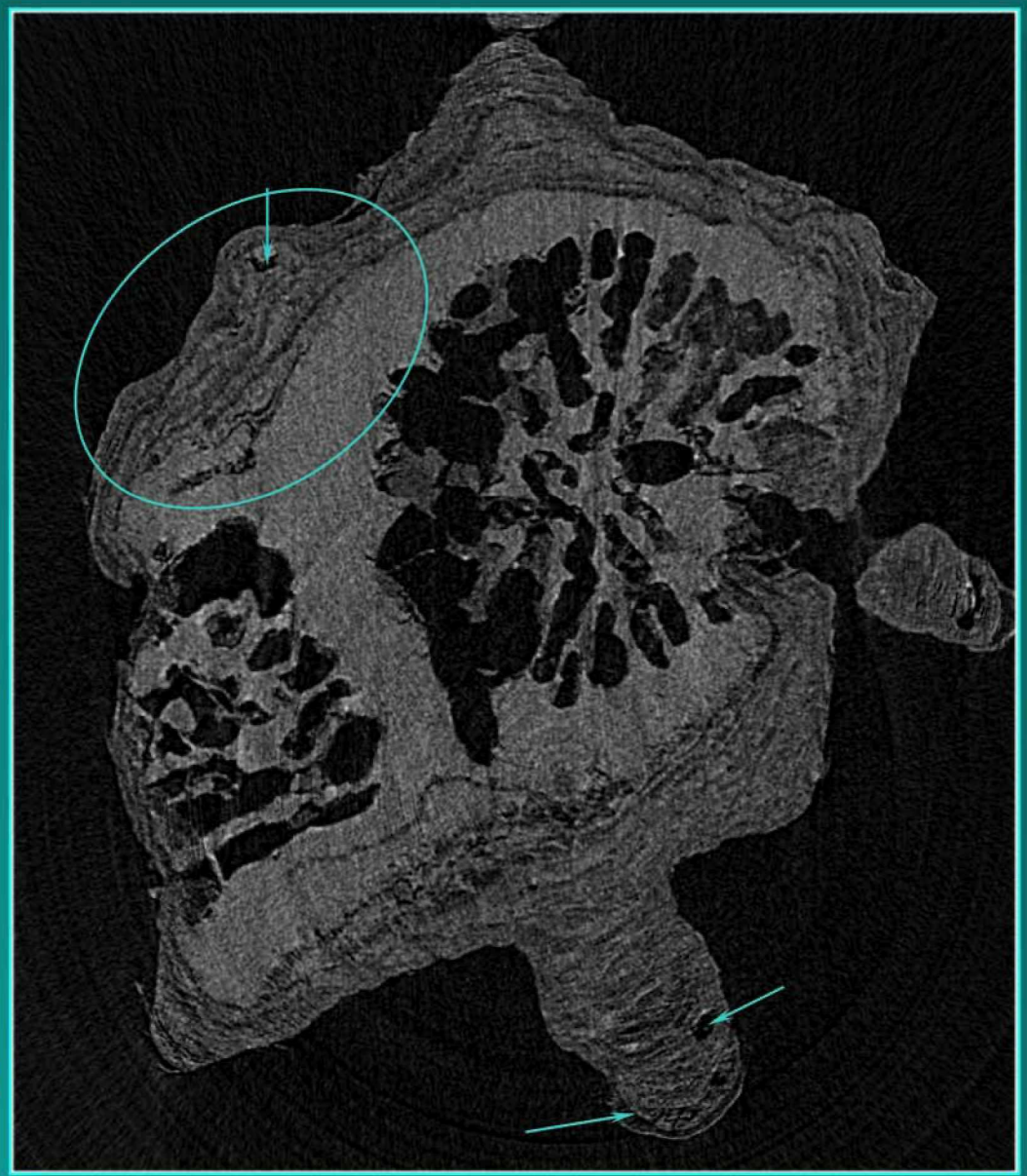

The succession of bands produced during the progressive calcification of the cell walls are visible
The identification of the reproductive organs immersed in the thallus (e.g. conceptacles), has allowed a correct determination of the life cycle of our specimen.

Courtesy of G.Bressan

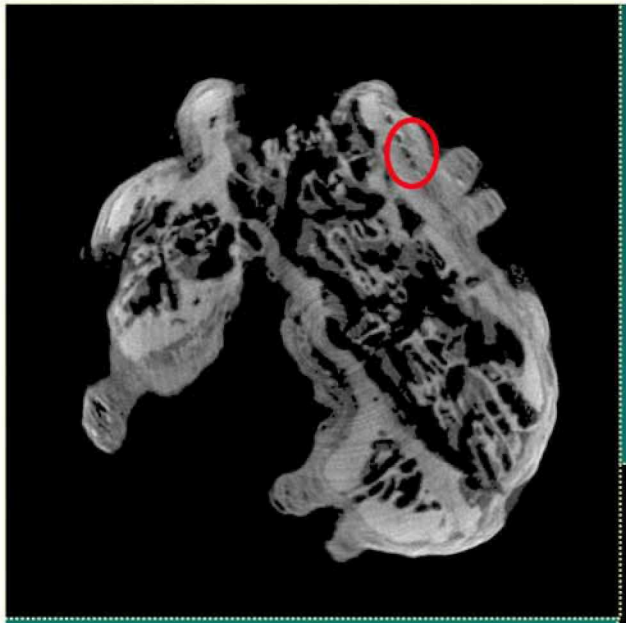

SEM image corresponding to a 100 μm x 80 μm area selected from one of the slices.
Layered distribution of diatoms (green circle), serpulids (yellow line), coralline algae (red line), cyanobacteries (blue line) clearly visible on border of this gallery.

Spatial and temporal sequence

EHT=15.00 kV WD= 28 mm Mag= 904 X
10μm Photo No.=4576 Detector= SE1

Courtesy of G.Bressan

Small cracks and defects in Aluminium Friction Stir Welding (FSW) samples

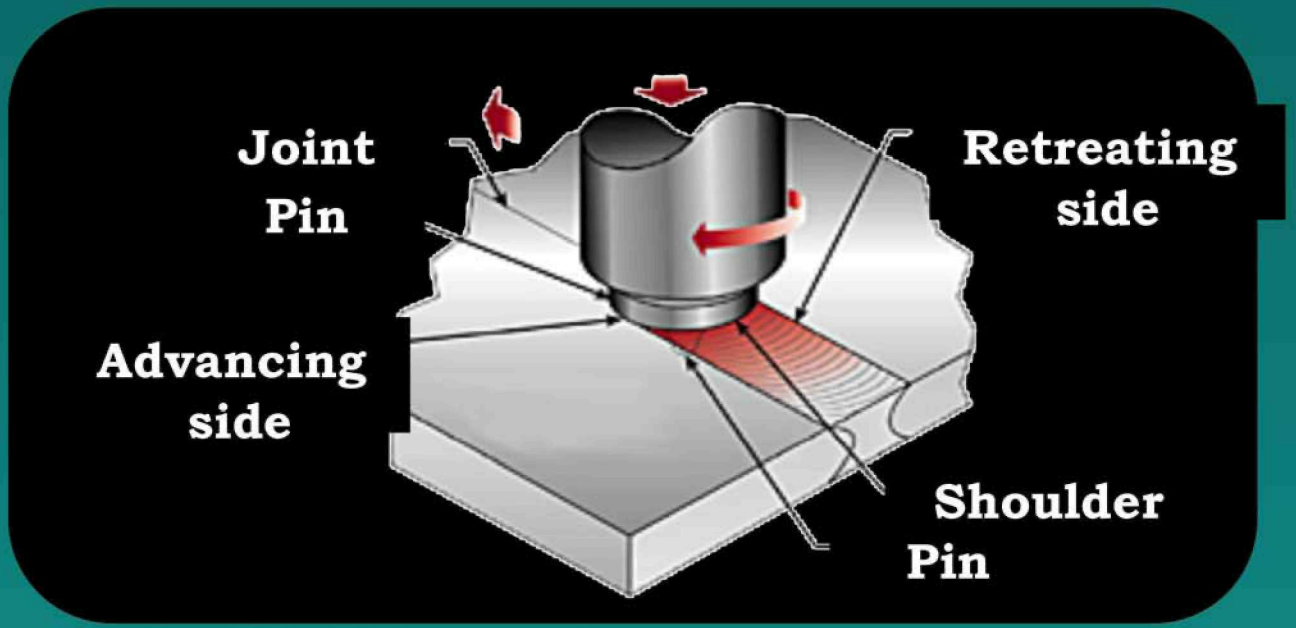

- high speed rotating tool
- frictional heat
- no melting
- plasticized material
- solid phase bond

high quality, no pores, uniform structure, small defects, very difficult to detect

A Definition of defects position and dimension in welded joints is very demanding for application of fracture mechanics techniques and improvement of industrial aceptance criteria

tomographic slices (distance 0.8 mm)

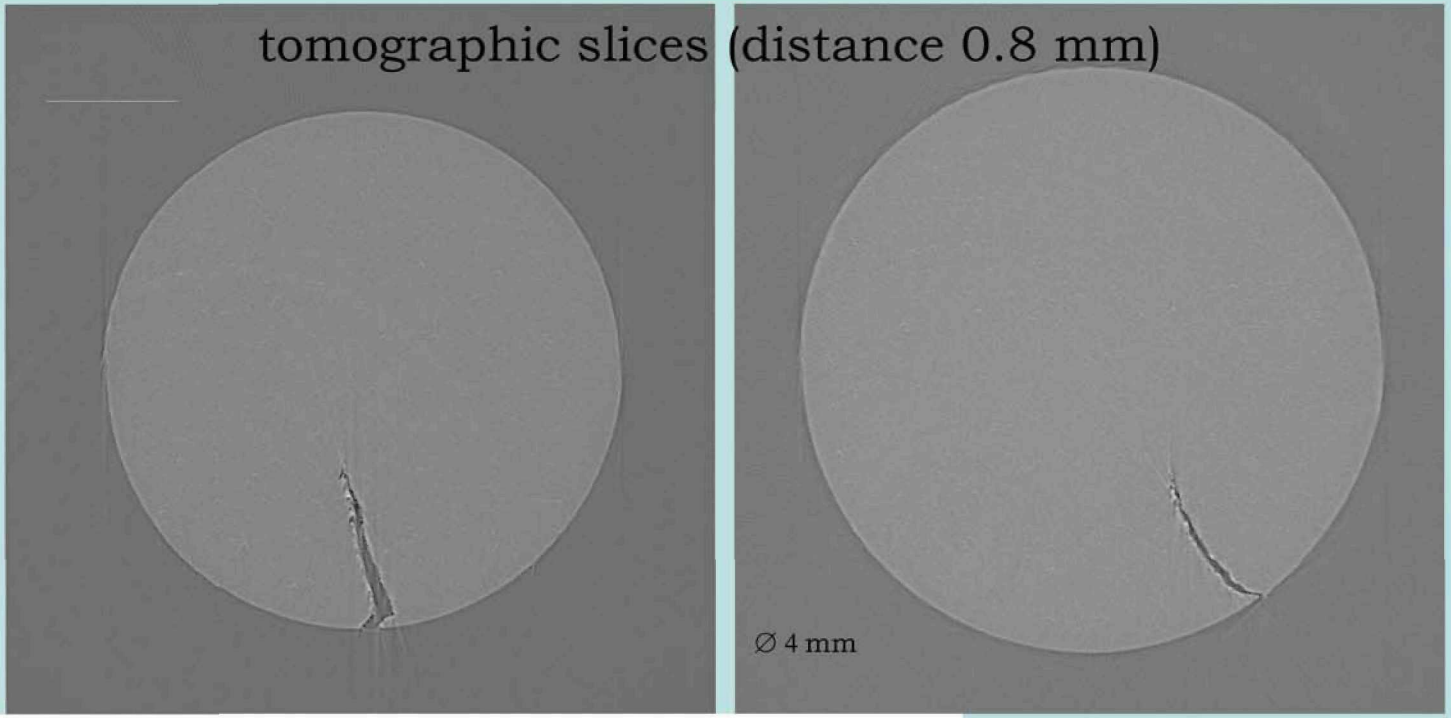

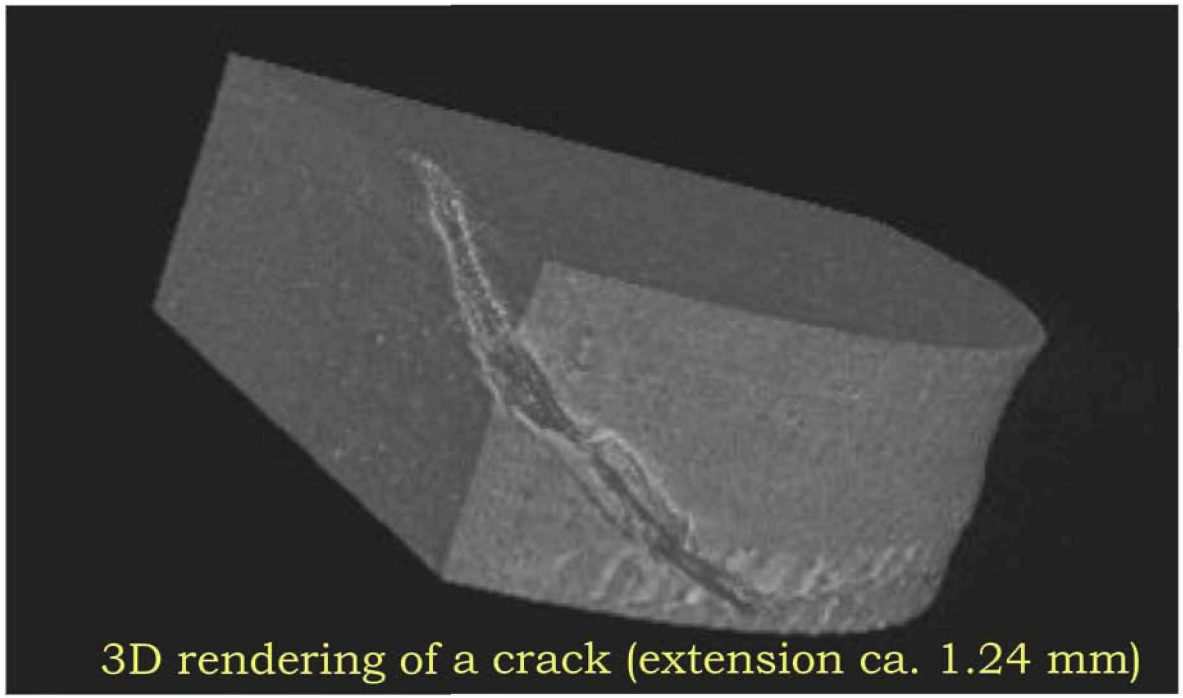

3D rendering of a crack (extension ca. 1.24 mm)

- Al notched sample subjected to torsion + bending

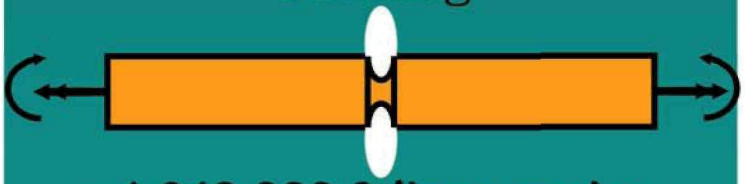

- 1.910.000 fatigue cycles
- CCD pixel size: 3.8 μm

F. Cosmi, et al.

3D crack model

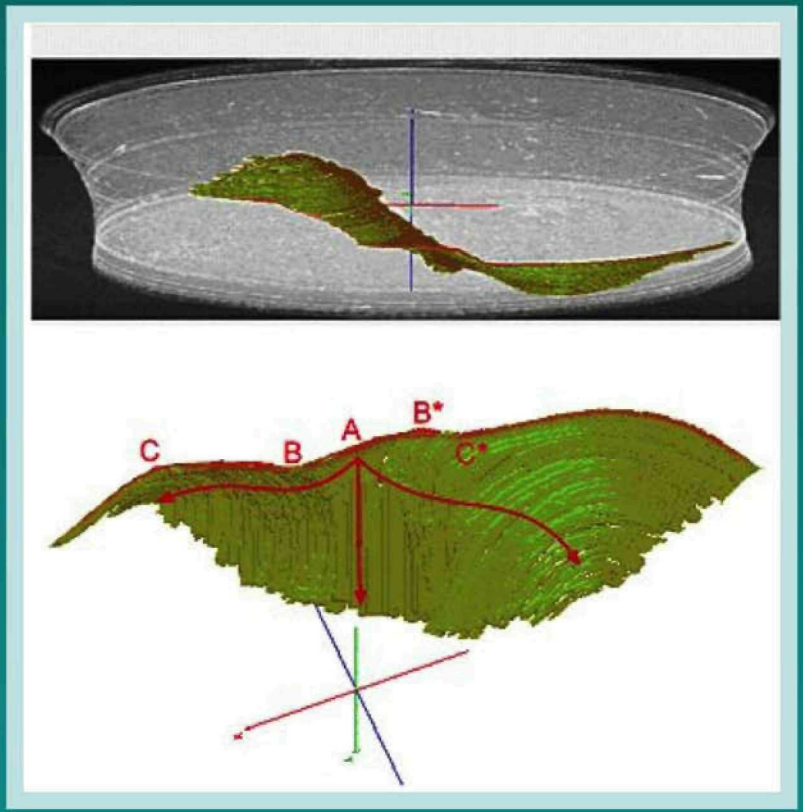

- software routine to trace the crack through the stack (by MATLAB)
- symmetric shape
  - nucleated in **A**
  - propagated in hoop direction until **B** and **B***
  - deflected until **C** and **C***
  - recovered the original direction
- surface of the crack composed of linear tracts

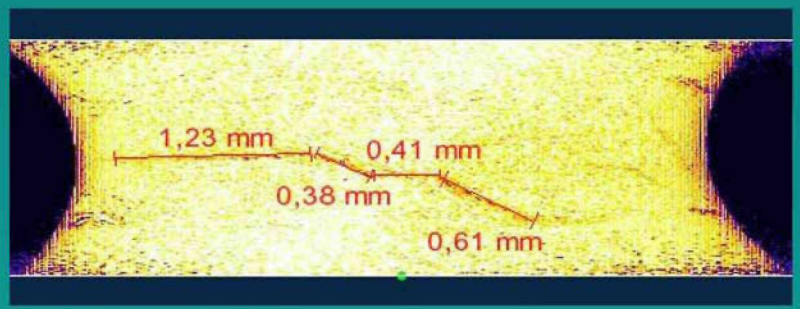

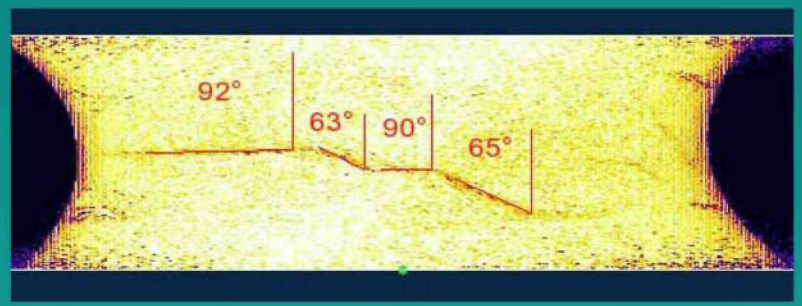

F. Cosmi, et al.

Study of porous media

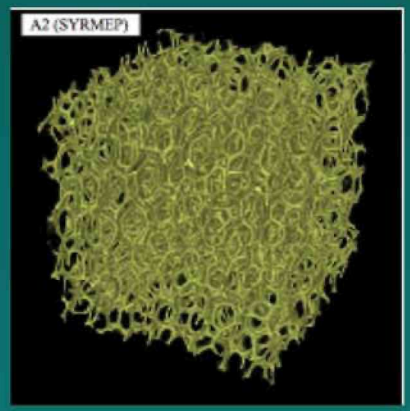

Porous media are very suited to be studied by PHC μCT

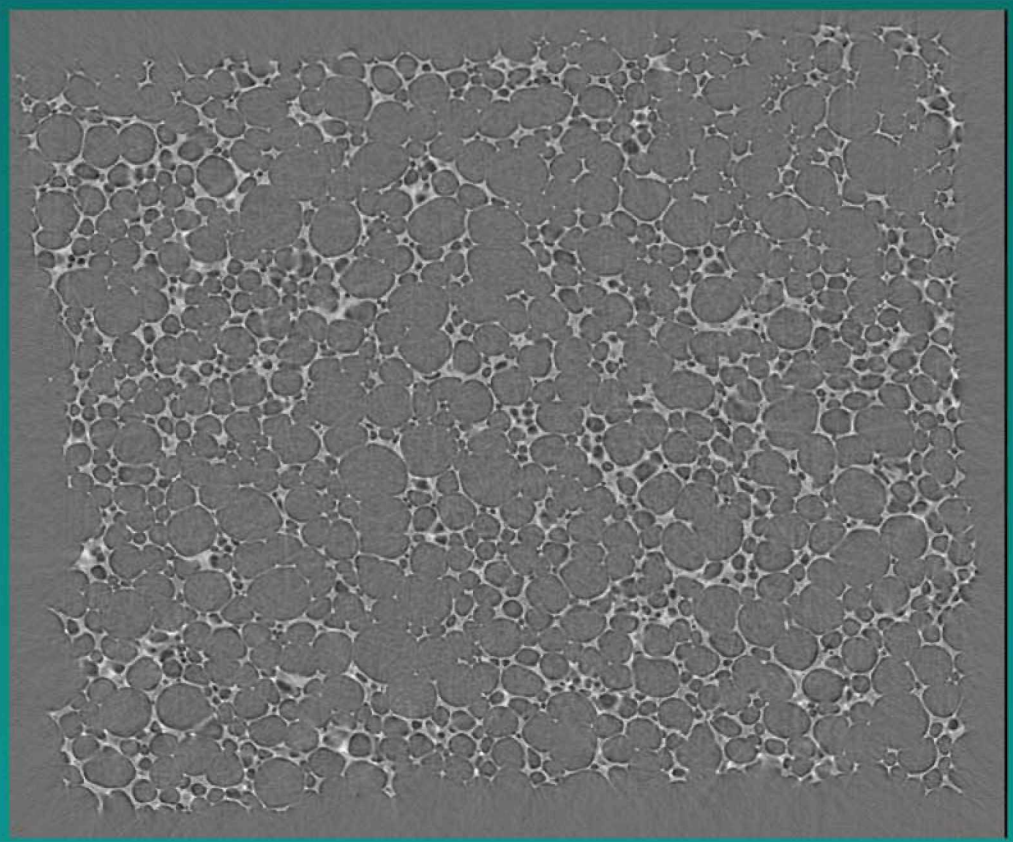

The study of porous media requires the knowledge of microscopic properties of the porous matrix, like: porosity, permeability, tortuosity, effective thermal conductivity, effective electric conductivity, etc.

The μ-CT scan and 3D volume rendering represent the first step which contributes to qualitatively explore the internal structure of the samples

A dedicated SW that perform filtering, segmentation, skeletonization, object counting, etc. have been developed for this purpose

Polyurethane foam used in the automotive industry

Study of trabecular bone structure by means of absorption μ−CT

- Osteoporosis causes alterations in the trabecular bone that produce a reduction of bone mass and density but also structural changes in the bone architecture.
- In general, the quantification of bone microarchitecture is mainly based on histology that allows to extract histomorphometric parameters quantifying bone structure in terms of shape and connectivity. This technique is destructive.
- Using μ-CT it is possible obtain a 3D digital map of the bone, to visualize the morphological structure and evaluate the main histomorphometric parameters.
- Using these data numerical methods can be applied to evaluate the elastic properties.

University of Bologna
Physics Department

ISTITUTI ORTOPEDICI RIZZOLI

elettra

High resolution μ-CT analysis of a proximal human femur with an innovative linear detector

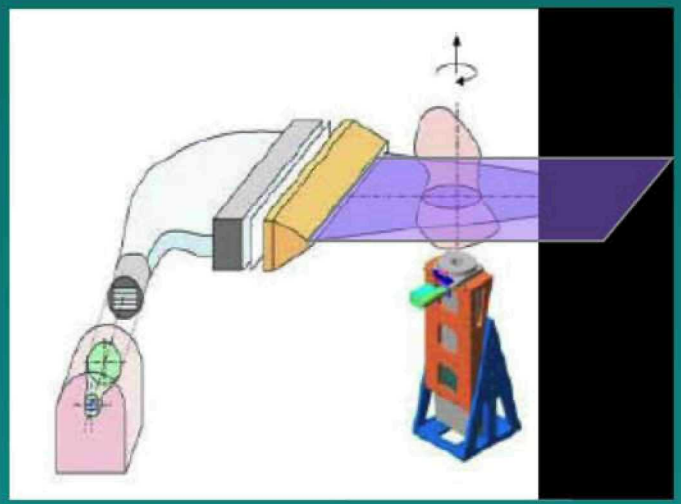

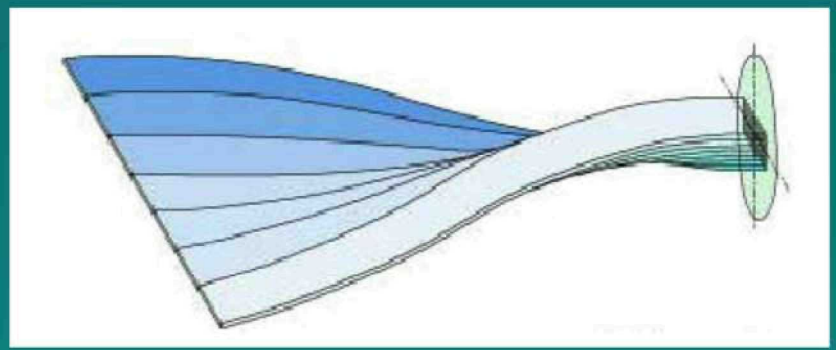

· Investigation of the **performance of a EBCCD-based system** with a nominal spatial resolution of 22.5 μm extended over a **FOV of 130 mm x 1 mm**.

• This system is obtained by using **a distinctive fiberoptic ribbon** (patented by the **University of Bologna**) converting a linear geometry to a rectangular one.

• A scan of **a 9 cm wide human proximal femur** allowed to analyze the trabecular structure of the bone in order to investigate changes caused by **osteoporosis**.

A. Pasini et al., Proceedings of IEEE NSS/MIC 2004 Annual meeting, Rome, Italy

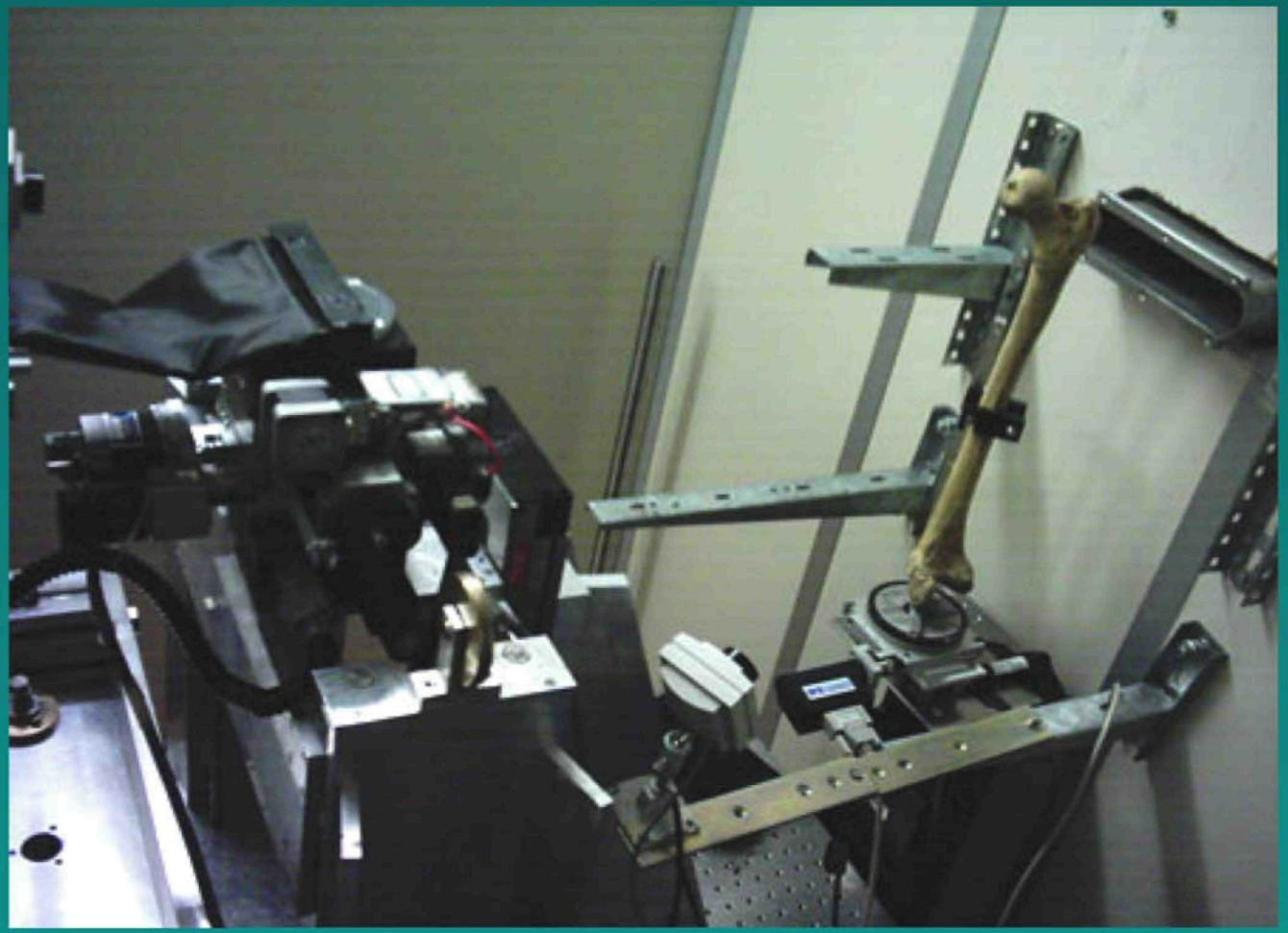

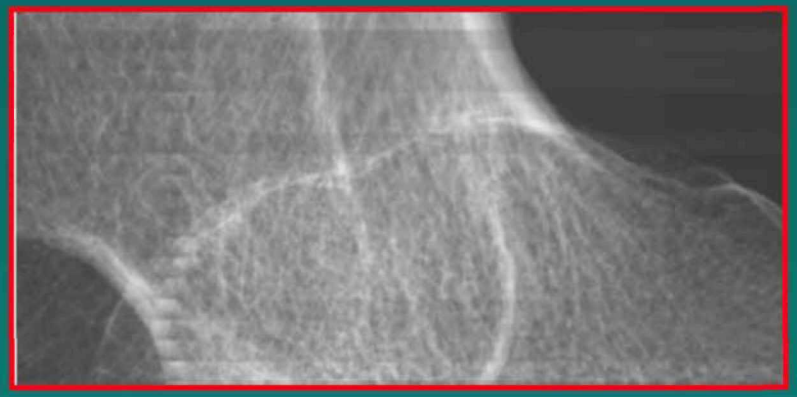

t_{exp} = 600 sec

E = 34 keV

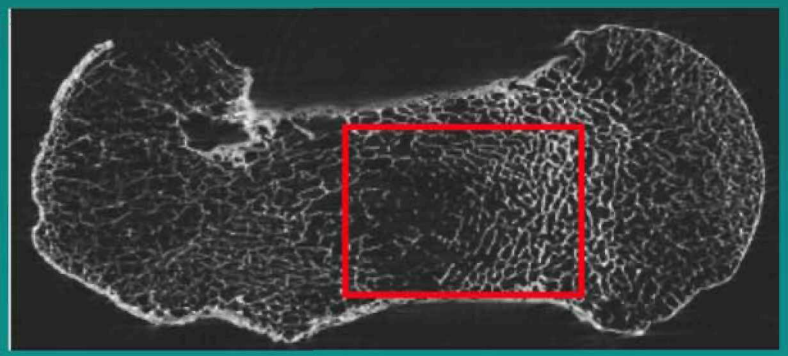

Reconstructed slice

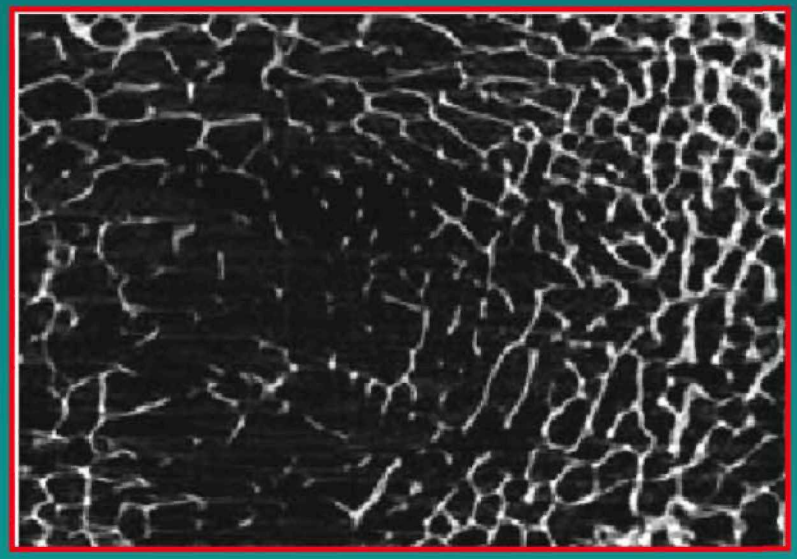

A. Pasini et al., Proceedings of IEEE NSS/MIC 2004 Annual meeting, Rome, Italy

University of Bologna
Physics Department

ISTITUTI ORTOPEDICI RIZZOLI

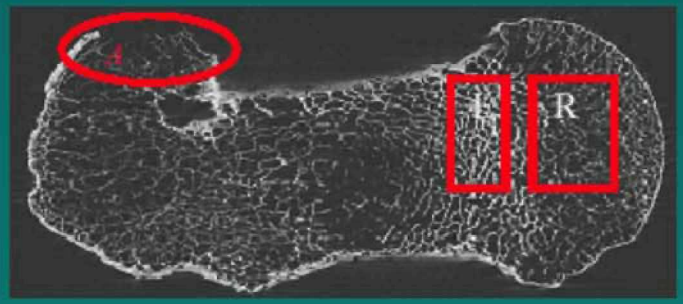

	BV/TV [%]	Tb.Th [μm]	Tb.N [mm^{-1}]	Tb.Sp [μm]
Left ROI	21.4±0.3	167±2	1.28±0.03	610±20
Right ROI	13.8±0.2	120±1	1.17±0.02	740±10

	BV/TV [%]	Tb.Th [μm]	Tb.N [mm^{-1}]	Tb.Sp [μm]
Big ROI	17.5±0.2	122±2	1.44±0.02	576±8

LEGENDA:
BV/TV – Bone Volume/Tissue Volume
Tb.Th – Trabecular thickness
Tb.N – Trabecular Number
Tb.Sp – Trabecular Space

Rendering of 50 slices

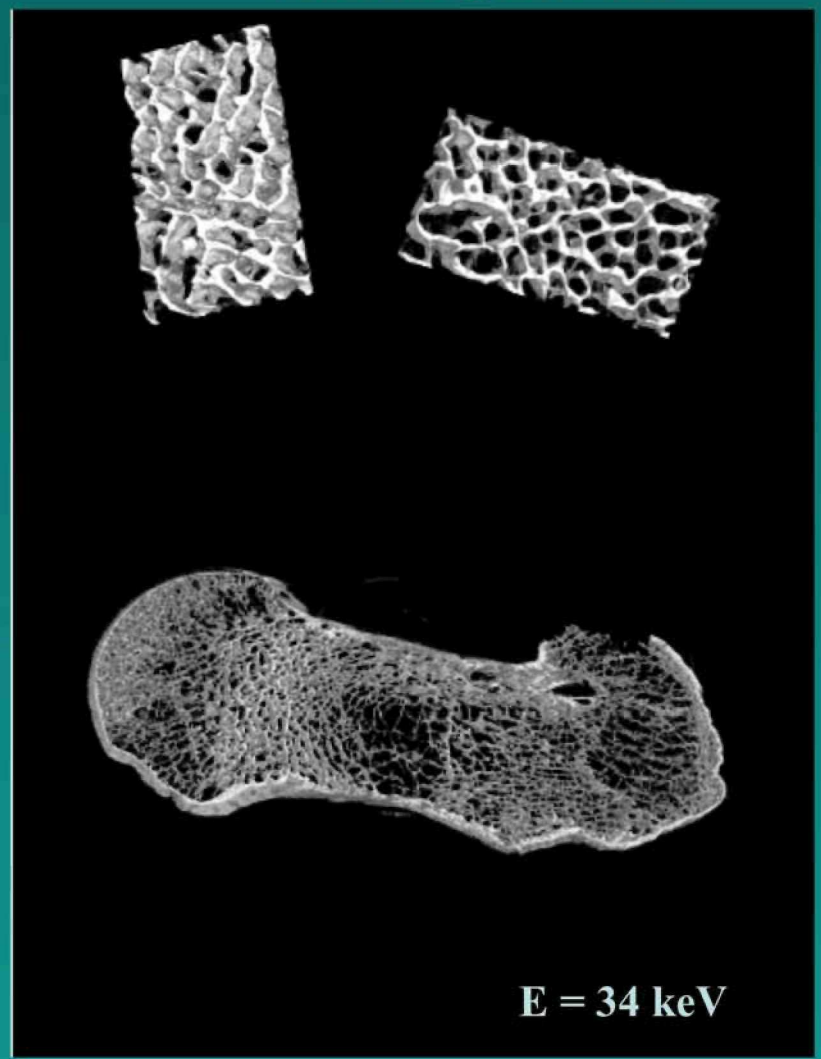

Imaging of archeological and recent wood

X ray μCT is a powerful tool for the anatomical investigation

Oak by optical microscope (cross section)

Oak by X ray μCT (SYRMEP beamline, 15 keV)

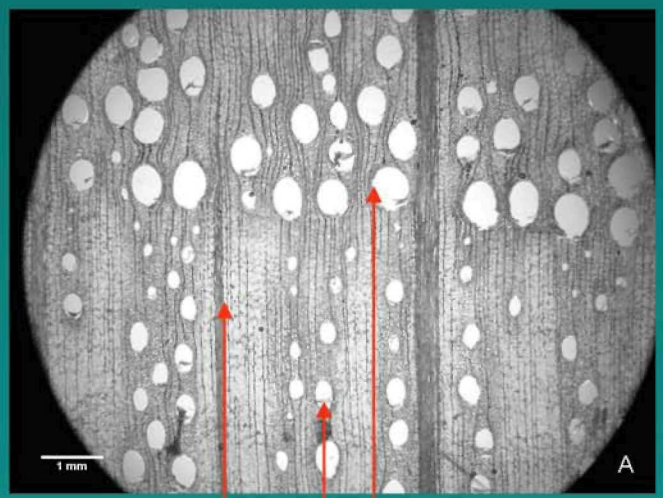

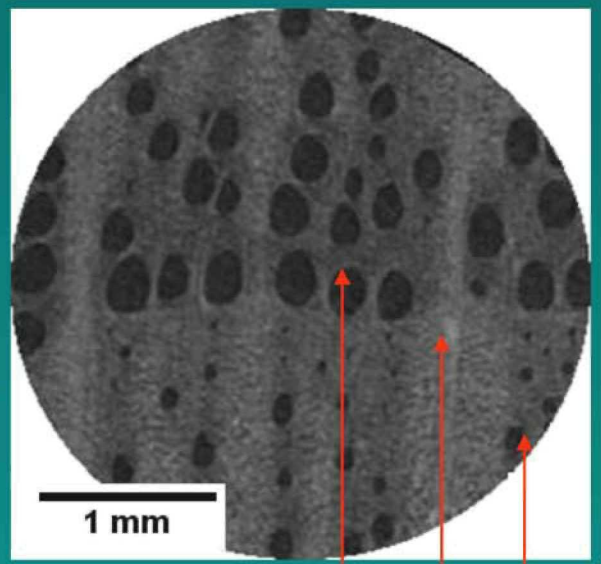

Spring Vessel (early wood)

Summer Vessel (late wood)

Parenchyma rays

Courtesy of N.Sodini

Spruce *(Picea abies)*

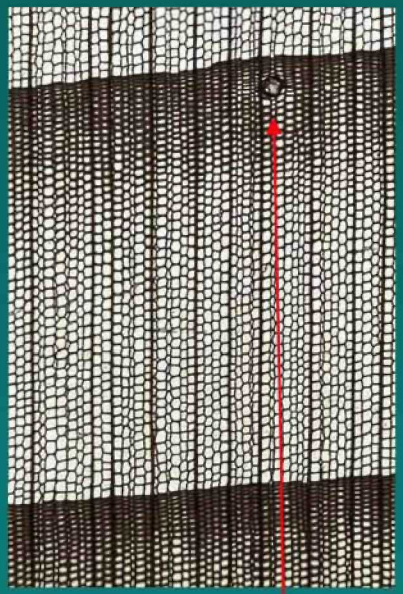

50X

Optical microscope

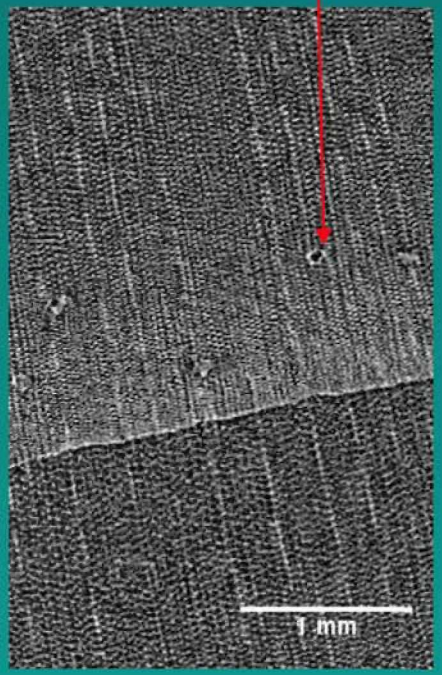

µCT images

European larch *(Larix decidua)*

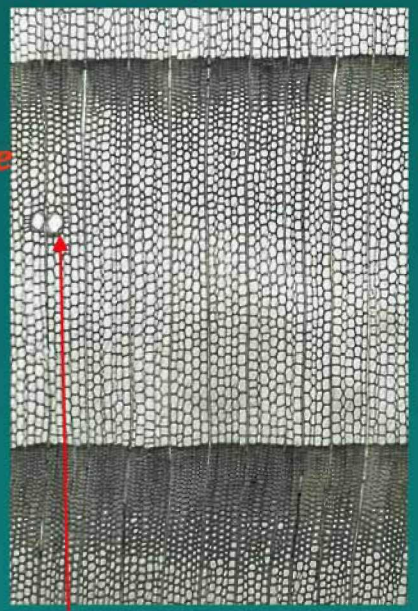

50X

Optical microscope

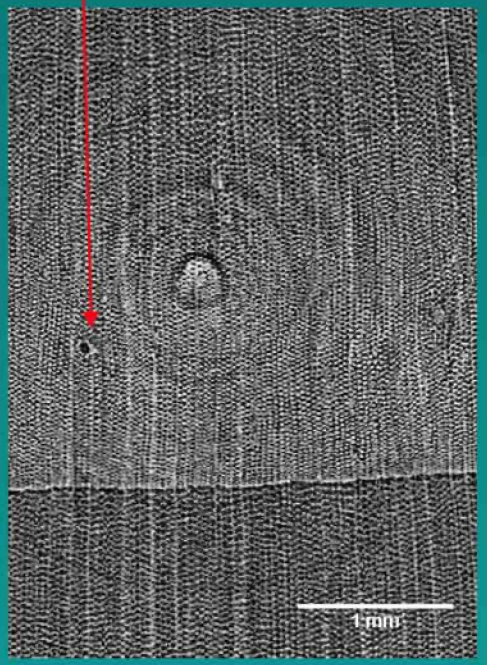

µCT images

Poplar *(Populus spp.)*

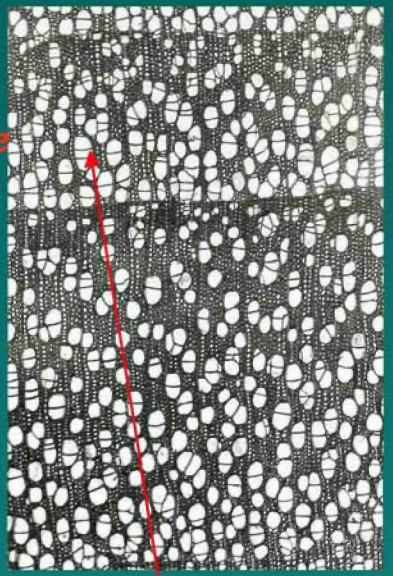

50X

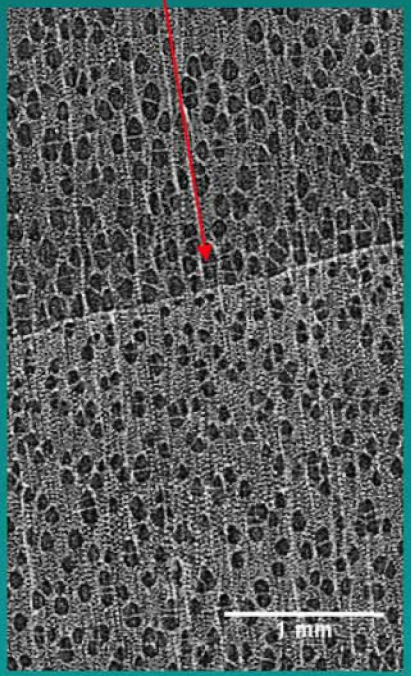

Archeological vs. recent oak

Archaeological oak

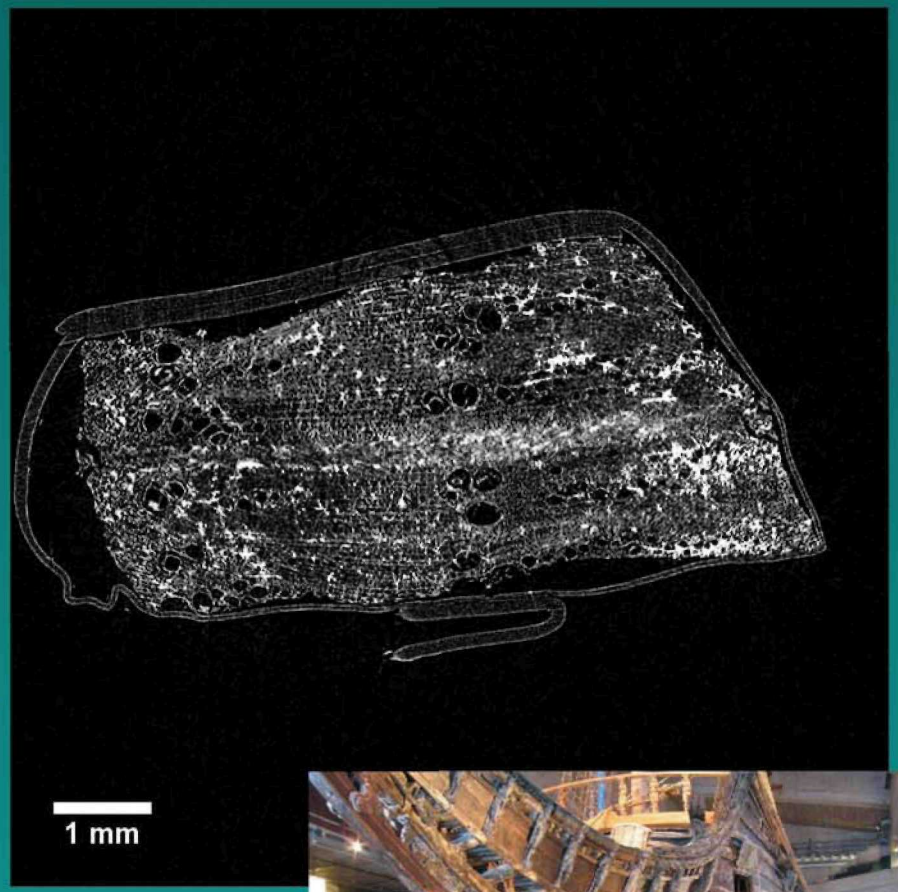

Recent oak

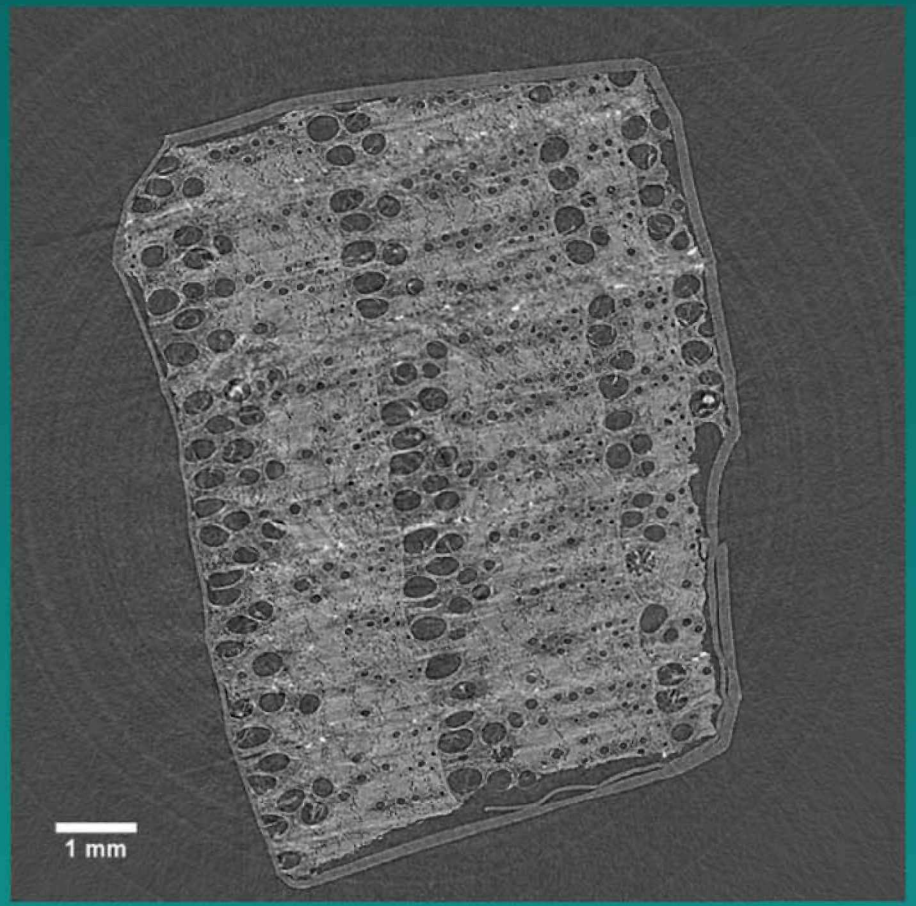

E = 15 keV

Courtesy of N.Sodini

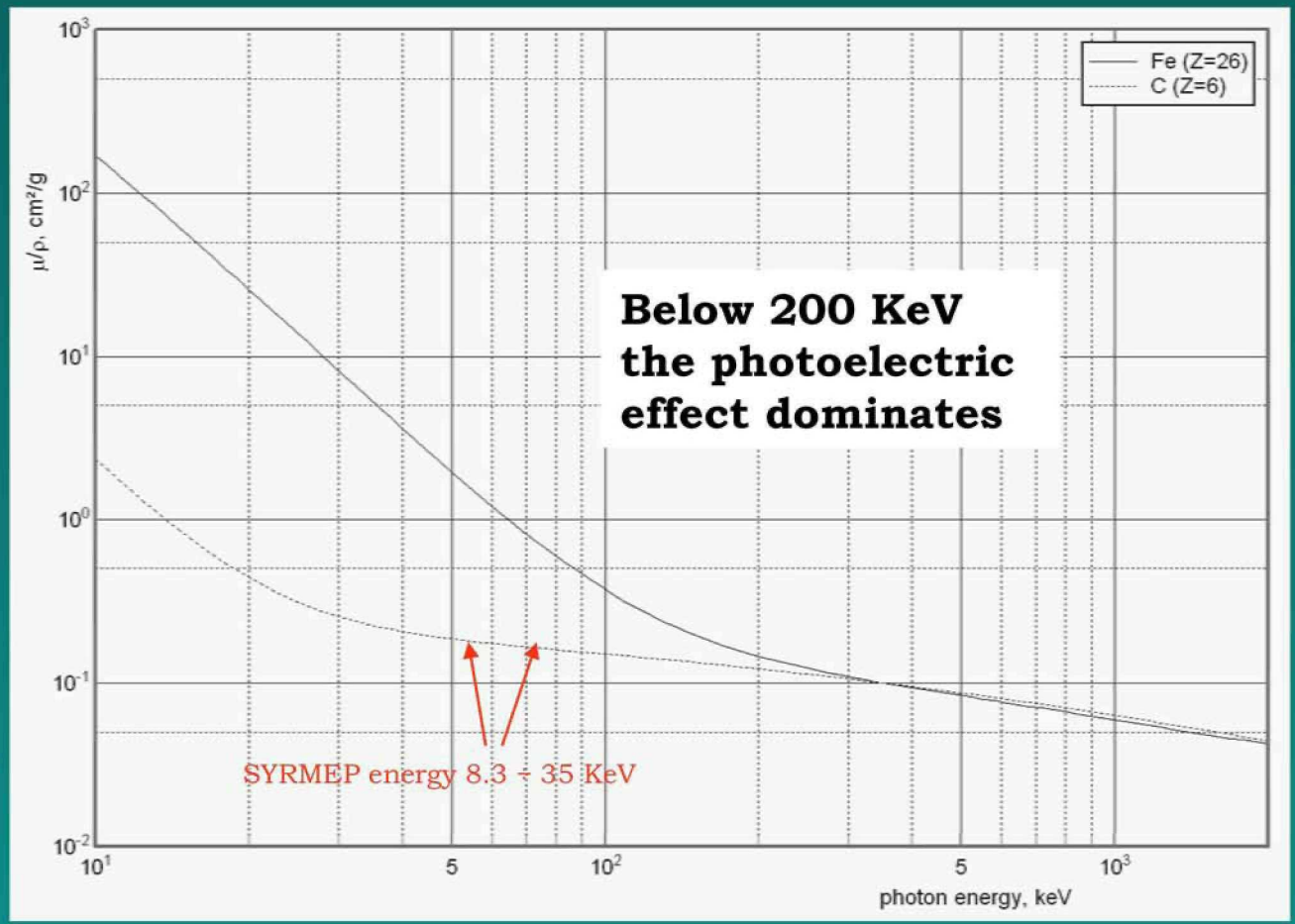

!!!

$$\frac{\mu}{\rho} = k\frac{Z^4}{E^3}$$

- a comparison of ρ between two areas or two sample can be done only in the case when Z is constant (same atomic element or same composition)

Courtesy of N.Sodini

Università degli Studi di Firenze

Calibration for measuring the μ(x,y)

elettra

Material	Chemical formula	Density (ρ) g/cm³	Mass attenuation coefficient cm²/g	Linear attenuation coefficient cm⁻¹
Propane liquid	C_3H_8	0.43	0.731	0.314
Acetone	C_3H_6O	0.789	1.048	0.827
Water	H_2O	1.00	1.674	1.674
Glycerol	$C_3H_5(OH)_3$	1.261	1.308	1.649
Chloroform	$CHCl_3$	1.483	15.93	23.624
Aluminum	Al	2.699	7.976	21.295

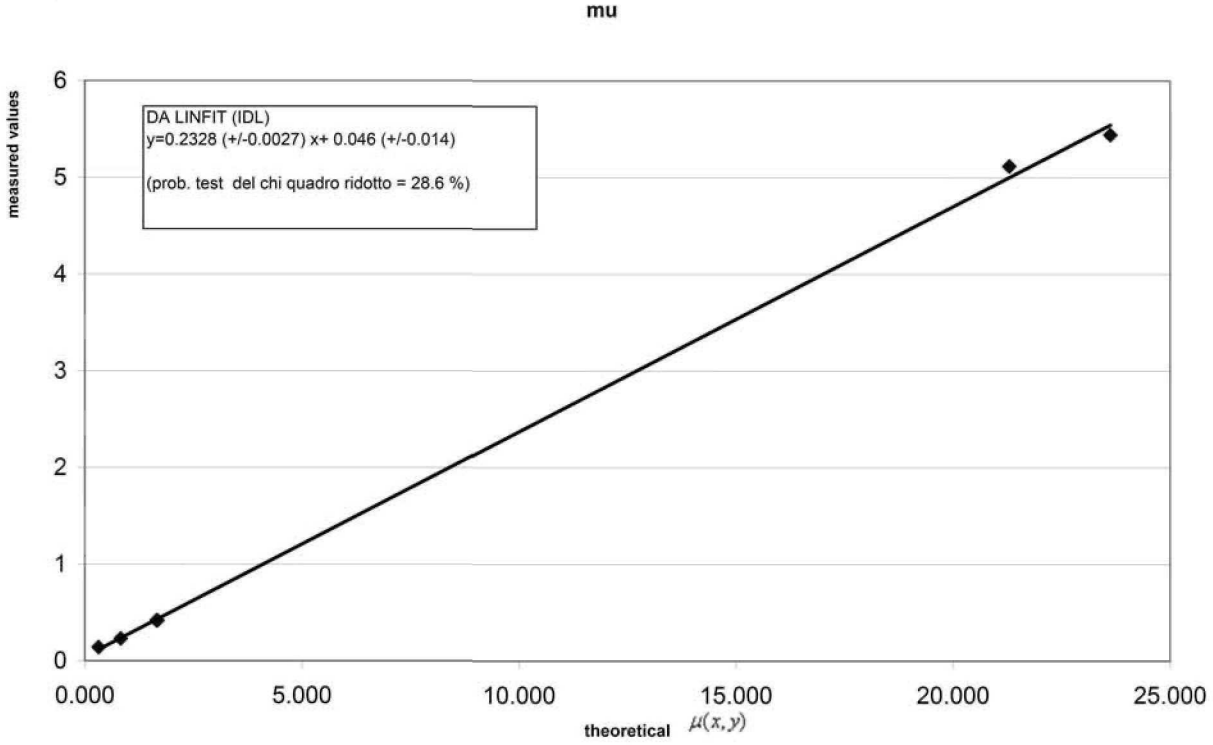

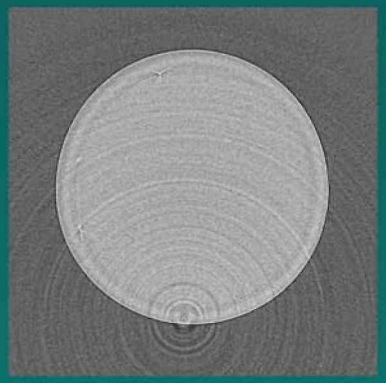

Acetone

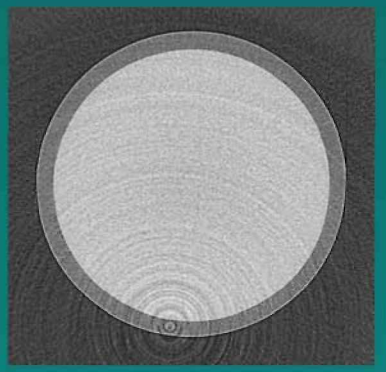

Glycerol

Aluminum

Experimental μ

vs theoretical μ

Courtesy of N.Sodini

Linear attenuation coefficient, μ(x,y), on recent and archaeological wood

Oak

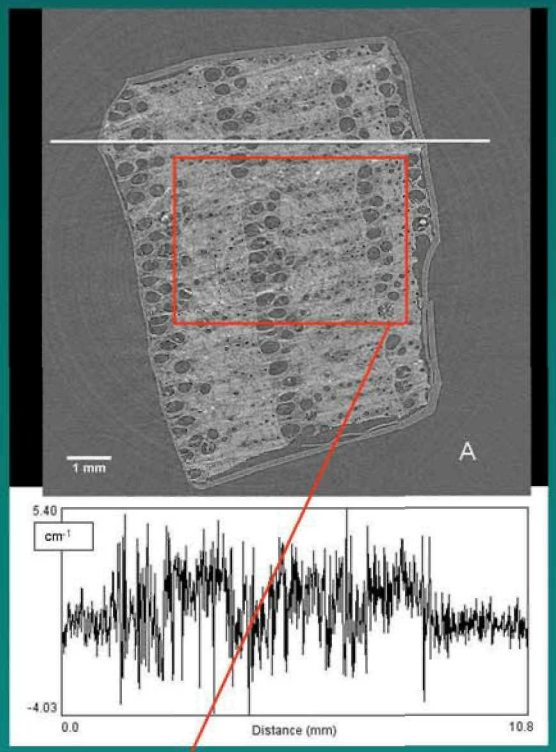

Average μ(x,y) value 1.27 cm^{-1}

Poplar

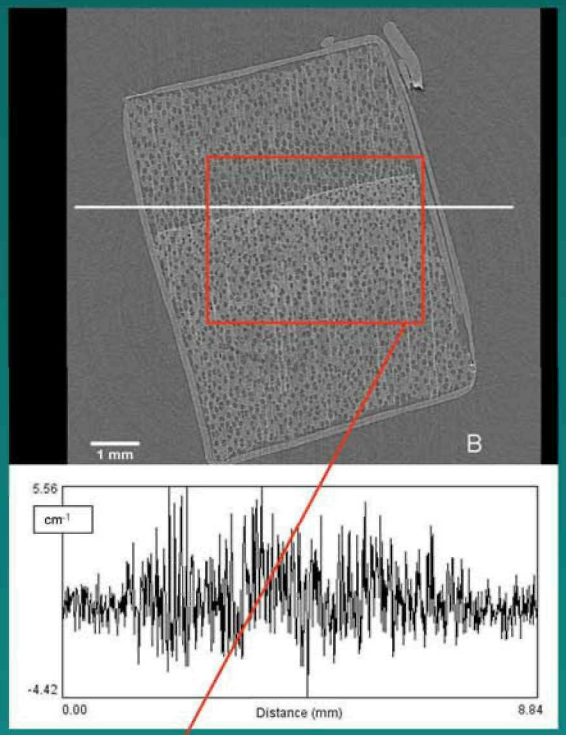

Average μ(x,y) value 0.44 cm^{-1}

Archeological oak

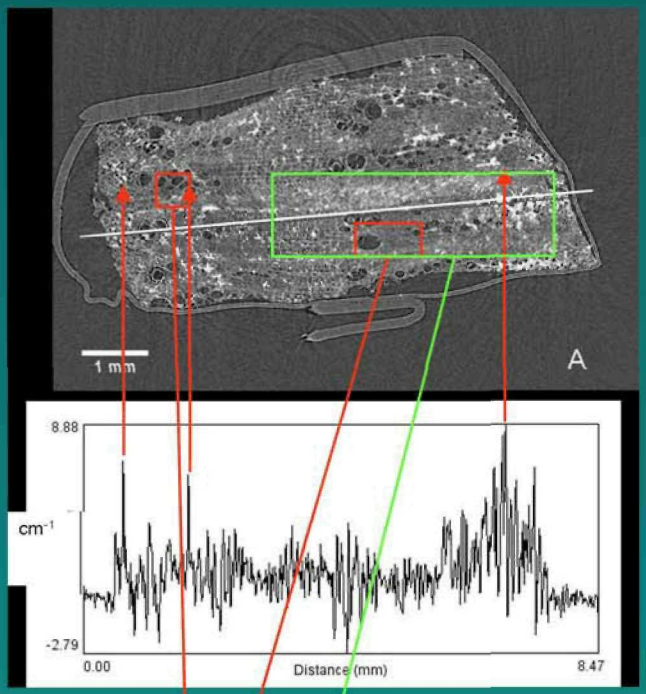

Average μ(x,y) values 0.79-0.93 cm^{-1}

Average μ(x,y) value 1.7 cm^{-1}

Courtesy of N.Sodini

From linear attenuation coefficient to Density

Normalization factor to obtain the μ value from the slices

$$y = 0.232x + 0.046$$

Experimental μ vs theoretical μ

at 15keV

$$K \Rightarrow x = \frac{y - 0.046}{0.232}$$

pixel value in the slice

$\mu_{(x,y)}$

Calculation of punctual density

$$\rho_{w_i}(x,y) = \overline{\rho}_w \frac{\mu_w(x,y)}{AVE(\mu_w(x,y))}$$

$\rho_{w_i}(x,y)$ = punctual density

$\overline{\rho}_w$ = average density of sample

$\mu_w(x,y)$ = punctual attenuation coefficient of wood

$AVE(\mu_w(x,y))$ = Average attenuation coefficient of wood

Courtesy of N.Sodini

Acknowledgement

to the SYRMEP team:

D.Dreossi, L.Mancini, E.Quai, R.H. Menk, N.Sodini, F.Zanini
Sincrotrone Trieste

F.Arfelli, E.Castelli, R.Longo, L.Rigon
University and INFN Trieste